Original Article

Institution of MECHANICAL ENGINEERS
Journal of MECHANICAL ENGINEERING SCIENCE

Proc IMechE Part C:
J Mechanical Engineering Science
0(0) 1–37

DOI: 10.1177/0954406220932208
journals.sagepub.com/home/pic
SAGE

Recent progress in flexibility effects on wing aerodynamics and acoustics

Prasert Prapamonthon[1,2], Bo Yin[1], Guowei Yang[1], Mohan Zhang[1,3] and Panpan Lu[1,3]

Abstract

Since the theoretical aeroelasticity for flapping-wing aerodynamics was introduced in the 1920s, the effects of flexibility on aeroelasticity have been paid more attention to aerodynamic design. In recent years, the trait of the wing flexibility is applied for small-scale wings of biomimetic flyers including micro air vehicles and mini unmanned aerial vehicles. Until now, the aerodynamic performance and great agility of these flyers, which are beneficially used for military missions and other civilian applications, have been improved through surrogate flapping wings with the favorable effects of the flexibility. As per the aeroelasticity principle for the forward flying, the chordwise flexibility of an elastic flapping wing can generate thrust and lift redistributions, whereas the spanwise flexibility can result in variations of the angle of attack and the shift of phase along the wingspan direction. Consequently, all vortices generated by the flapping wing i.e. (1) leading-edge vortices, (2) tip vortices, and (3) trailing-edge vortices are blended supportively, thereby improving the aerodynamic performance and agility. Hence, the growth of research and development of the aerodynamic performance and agility for these flyers under the influence of flexible wings increases through experimental and computational studies dynamically and rapidly. This review aims to highlight the important role of the flexibility in the recent progress in wing aerodynamics of these flyers through several wing models done by famous groups of experts in this field. In addition, this review includes the acoustics of the wings under the flexibility effects which is considered as a new key for better flyer design and improvement. A comprehensive understanding of the integrated aerodynamics and acoustics under the wing flexibility is, therefore, needed.

Keywords

Flexibility, wing, lift, propulsion, acoustics

Date received: 27 November 2019; accepted: 13 May 2020

Introduction

Since the theoretical aeroelasticity for flapping-wing aerodynamics was introduced by Birnbaum in the 1920s,[1] the effects of flexibility on aeroelasticity have been paid more attention to aerodynamic design. In recent years, the trait of the wing flexibility is applied for small-scale wings of biomimetic flyers including mini unmanned aerial vehicles (MUAVs), and micro air vehicles (MAVs). The continuous progress in the development of the aerodynamic performance and agility of these flyers, which are beneficially used for military missions and other civilian applications, has been done through surrogate flapping wings with the favorable effects of the wing flexibility.[2–14] Recently, research and development of the aerodynamic performance, agility, and flow mechanism associated with flexible wings of these flyers have been investigated dynamically, increasingly, and extensively.[14–33] In fact, according to insect flights, the small size and light weight of flyers are designed. Wings of the flyers usually fly at low speeds and the airflow associated with this flight is in the region of low Reynolds numbers (Re $\sim 10^3$). In this region, it is found that the formation, shedding, and combination of leading-edge vortices (LEVs), trailing-edge vortices (TEVs) as well as tip vortices (TVs) play important roles in lift and thrust generated by the wing.[4,33] Some

[1]Key Laboratory for Mechanics in Fluid Solid Coupling Systems, Institute of Mechanics, Chinese Academy of Sciences, Beijing, China
[2]Department of Aeronautical Engineering, International Academy of Aviation Industry, King Mongkut's Institute of Technology, Ladkrabang, Bangkok, Thailand
[3]School of Engineering Science, University of Chinese Academy of Sciences, Beijing, China

Corresponding author:
Bo Yin, Key Laboratory for Mechanics in Fluid Solid Coupling Systems, Institute of Mechanics, Chinese Academy of Sciences, No. 15 Beisihuanxi Rd, Beijing, 100190, China.
Email: yinbo@imech.ac.cn

studies[34,35] indicated that lift may be increased by the presence of LEVs. Moreover, in this flow region, flights of the flyers are likely to be sensitive to wind gusts. These circumstances lead to overall complex fluid–structure interactions of the flyers and typical designs of flyers with fix wings encounter fundamental challenges in the limitation of propulsion and aerodynamic performance such as lift generation including problems of flight mechanics and its control.[4,5,15,26,28] With the interest in overcoming these obstacles, flapping-wing models with the favorite effects of the flexibility are proposed. Typically, a flapping wing is a thin aerofoil which contains a flexible structure, thereby tending to deform during flight.[4,33] Hence, characteristics of biological flights are often observed and investigated to improve the aerodynamic performance, agility, wing structure, mechanics of flight and control, including propulsion of wings of the biomimetic-flyer wings, MUAVs, and MAVs for desirable mission achievements.[4,13,14,19,24,30] However, the wing of biological flyers is anisotropic and cambered.[36] Specifically, its flexibility is different in the spanwise and chordwise directions.[22,37–42] The elastic stiffness in the chordwise direction has a square correlation with the chord length and the elastic stiffness in the spanwise direction has a cube correlation with the wingspan. Thus, it seems likely that the trend of the wing deflection of larger insects may occur easier in the chordwise direction.[37] The flexibility of the wing may have a great impact on aerodynamic performance and the flexible wing typically deforms under the integrated effects of aerodynamic force and wing inertia.[43] It was shown in the open literature[7,9–11] that both wing flexibility and rigidity are increased by wing corrugation and the large wing flexibility causes more complicated phenomena of fluid–structure interactions around a wing. In fact, a large-flexible wing seems unreasonable and unsuitable because it is easy to damage from buckling caused by the compressive load from fluid–structure interactions during flight.[4] Consequently, the kinetics and kinematics of a highly flexible wing during flapping motion cause highly coupled nonlinearities in the calculation of aerodynamics, aeroelasticity, dynamic and feedback controls of flight.[4,44] Further, to approach the real fight of insects and obtain the benefit of the insect flight, the characteristics of the wing acoustics of flying insects need to be investigated. A new trend of the flapping-wing design indicates the high aerodynamic performance of these flyers should be achieved with low noise[32] since it might be important in some applications of biomimetic flyers such as reconnoitering in a military mission. Although the flapping-wing sound has been studied for ages, most models are rigid. Very little attention to the importance of the flexibility effects on the wing acoustics of a flyer during flight has been given, so far. Some studies have been highlighted by some groups of researchers.[32,45–47] Based on a literature review, although several questions in flexible-wing effects on aerodynamics are addressed, there are still several interesting questions about the aerodynamic performance and aeroacoustics of biomimetic flyers, MAVs, and MUAVs under the influence of the wing flexibility which needs to be adequately addressed to answer the unknown question whether the structural deformation caused by the flexibility effects really provides aerodynamic and propulsive advantages as well as a favorable impact on sound generation and propagation or not. It suggests that the role and importance of the flexibility should be specified clearly for the design improvement of these flyers. In a previous comprehensive review on the aerodynamic and aero-elastic characteristics of rigid and flexible wings in several flying motions done by Shyy et al.[4] they raised some useful questions about the flapping-wing aerodynamic performance under the flexibility effects, for example, How do the effects of geometrical nonlinearity and the anisotropic structure result in the flapping-wing aerodynamics? and How can the stability of flapping flights be improved passively via the favorable effect obtained from flexible structures? These questions still need to be explained more. To accomplish the missions in practice for recent years, other research questions about aerodynamics and aeroacoustics under the flexibility effects need to be addressed as well. For example, it is thought that the flexibility is likely to be a key factor for aerodynamic and aeroacoustic improvements, so the flexible wing has a greater impact on aerodynamics and aeroacoustics than the rigid one, especially when a highly flexible flapping wing is used. Therefore, (1) How can lift and thrust be improved significantly not only during hover and forward flight but also in turning flight? (2) How can buckling effect be reduced passively if a flyer is under given compressive loads? (3) How can optimal flexibility be done to attain high aerodynamic performance and low noise? (4) How is the mechanism of the sound generation and propagation under different direction flights? (5) Does noise generated by insects relate to aerodynamic load and How? Since all of the above questions are linked inherently, a comprehensive understanding of the mechanism, functionality, and influence of the flexibility on flapping wings, including sound generation is essential. Specifically, the effects of flexibility on kinematics, aerodynamics, and acoustics need to be addressed for the success of future designs of flexible flapping-wing flyers. As open literature cited in the references, three main concerns of flight improvement of biomimetic flyers, MUAVs and MAVs are described. One is wing lift which is an aerodynamic force for holding a flyer in the air. The next one is flying thrust which is used to move a flyer forward through the air. Lastly, aeroacoustics generated by flapping-wing motion which is usually related to the lift and thrust of the flyers. This paper aims to review, conclude, and complement recent works in the effects of the flexibility on

wing aerodynamics and acoustics. The authors hope that this paper will be helpful information for the community and encourage future reviews and research efforts. The following parts of the paper are organized as follows: the governing equations for flapping kinematics, important dimensionless numbers as well as key variables in flexibility are presented in Coordinate systems, parameters, and equations of flapping wing control section. The wing aerodynamic performance under the flexibility effects, which are presently considered in the open literature, is updated in Effects on wing aerodynamic performance section. Effects on wing acoustics section further reviews the effects of the flexibility on wing acoustics generated by biomimetic flyers as well as its propagation physics. Finally, some recommendations for future study and conclusion are provided in Recommendation section.

Coordinate systems, parameters, and equations of flapping wing control

This section introduces the coordinate systems, important kinematic parameters, and equations that are needed for the flapping-wing motion modeled for the unsteady flow. The kinematic equations, Navier–Strokes equations, and the nonlinearity with multiple variables i.e. velocity and pressure as well as moving geometries are mentioned. Some nondimensional numbers which are used to characterize the flight regime of a flyer are described also. Also, the plate-deformation equation for in-plate and out-of-plate motions is added to introduce the effects of flexibility, including related variables such as effective stiffness.

Coordinate systems and kinematic parameters of flapping flight

Basically, kinematics of a complex flapping-wing flyer can be modeled by the kinematics of a rigid body and wingbeat coordinate systems. As shown in Figure 1(a)–(c), the body angle (χ) is used to describe the rigid body. At the same time, the wing kinematics is represented by three independent angular positions within the stroke plane: (1) the flapping angle (ϕ) used to describe the flapping motion about the x-axis, (2) the angle of attack (α) used to describe the rotation about the y-axis, and (3) the elevation angle (θ) used to describe the rotation about the z-axis. The horizontal plane is the plane parallel to the ground. The stroke plane, shown in Figure 1(d), is defined by three points: wing root or base (point O), and the angular positions of wing tip at the maximum and minimum for points $W_{T,A}$ and $W_{T,B}$, respectively. During the hovering flight, the stroke plane is near horizontal but it is near vertical in the forward flight. The stroke plane angle or stroke angle (β) is ranged from 0° to 90° for hovering and forward flights, respectively. The body angle and stroke angle also vary when flyers are in the flight mode. Moreover, the stroke plane could change considerably in the spanwise direction during the flight due to the wing deformation from torsion, causing the torsional angle (γ). Besides, the angle of attack is used to define the angle between the stroke plane and the chordwise-strip wing, as seen in Figure 1(e) and 1(f) for the upstroke and downstroke attack angles, respectively.[15] All mentioned kinematic parameters are summarized in Table 1.

For a general 3D case, the following equations based on the Fourier series are used to describe the wing kinematics i.e. the flapping angle, the elevation angle, and the angle of attack.[48] The unit of all the angles is in radian.

$$\phi(t) = \sum_{n=0}^{3} \left[\phi_{c,n}\cos(n\omega t) + \phi_{s,n}\cos(n\omega t)\right] \tag{1}$$

$$\theta(t) = \sum_{n=0}^{3} \left[\theta_{c,n}\cos(n\omega t) + \theta_{s,n}\cos(n\omega t)\right] \tag{2}$$

$$\alpha(t) = \sum_{n=0}^{3} \left[\alpha_{c,n}\cos(n\omega t) + \alpha_{s,n}\cos(n\omega t)\right] \tag{3}$$

$$\alpha_{in}(t) = \sum_{n=0}^{3} \left[\alpha_{in,c,n}\cos(n\omega t) + \alpha_{in,s,n}\cos(n\omega t)\right] \tag{4}$$

$$\alpha_{out}(t) = \sum_{n=0}^{3} \left[\alpha_{out,c,n}\cos(n\omega t) + \alpha_{out,s,n}\cos(n\omega t)\right] \tag{5}$$

where $\omega = 2\pi f$, f is the flapping frequency, t is the time, and n = 0, 1, 2, or 3. The coefficients $\phi_{c,n}$, $\phi_{s,n}$, $\theta_{c,n}$, $\theta_{s,n}$, $\alpha_{(c,n)}$, and $\alpha_{(s,n)}$ are Fourier coefficients which are determined from empirical kinematic data as reported in the references.[49–51] Terms α_{in} and α_{out} represent the attack of angles at the wing tip and at the wing base/root based on the inner and outer cross section of the wing and the forewing, respectively.[19] An example of the variations of the angle of attack (α), elevation angle (θ), and flapping angle (ϕ) for one period of a real wing of hawkmoth hovering are plotted in Figure 2(a). It shows the first order of a sinusoidal curve of the flapping-angle variation approximately. The elevation-angle variation also shows like the first order of a sinusoidal curve with low amplitudes and twice the frequency of main flapping frequency. Differently, the angle of attack shows asymmetric patterns per stroke with a phase lead about 90° from the flapping angle.

To simplify the kinematics of the real wing, the flapping and attack angles within the stroke plane may be governed by simple harmonics wing motion (SHWM), which defined by a sinusoidal function with the same frequency and the same or different phase. This may be reasonable because the elevation angle is

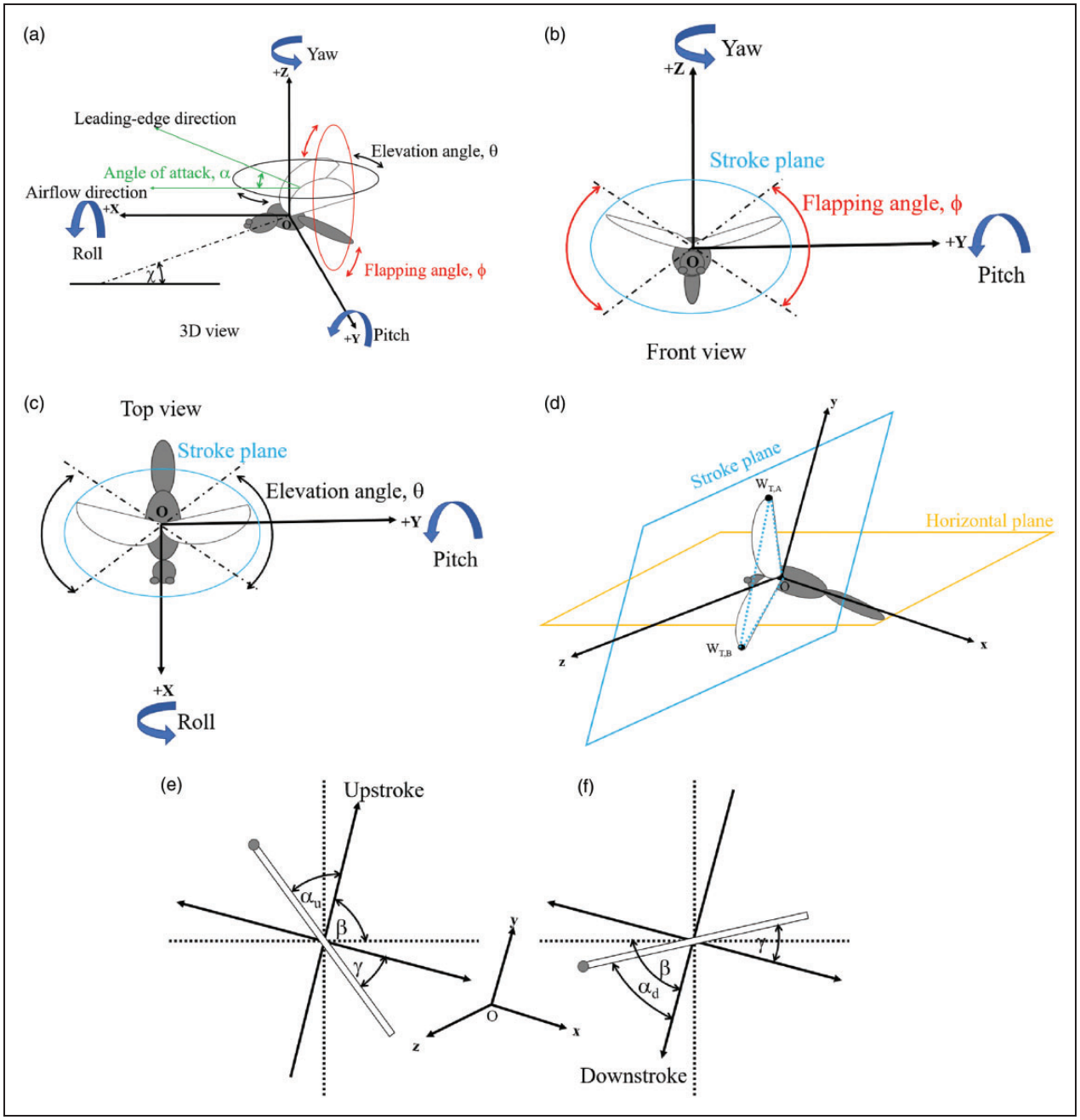

Figure 1. 3D diagram of coordinate systems used to describe kinematics of body and flapping wing motions.

assumed to keep unchanged as its magnitude is small, thereby causing a low effect on the mean lift and drag forces. Thus, the effect of the elevation angle is ignored.[19,52,53] Consequently, a simplified flapping wing can be described by the following equations.

$$\phi(t) = \phi'_{c,1}\cos(\omega t) \tag{6}$$

$$\theta(t) = 0 \tag{7}$$

$$\alpha(t) = \alpha'_{c,1}\sin(\omega t) \tag{8}$$

$$\phi'_{c,1} = \sqrt{\phi^2_{c,1} + \phi^2_{s,1}}, [50] \tag{9}$$

$$\alpha'_{c,1} = -\left(\frac{\sqrt{\alpha^2_{out,c,1} + \alpha^2_{out,s,1}} + \sqrt{\alpha^2_{in,c,1} + \alpha^2_{in,s,1}}}{2}\right) \tag{10}$$

Equation (10) is used in the reference,[54] the variations of the angle of attack, the elevation angle, and the flapping angle of the simplified wing for one period can be presented in Figure 2(b). However, based on SHWM and unsteady flow, the angle of attack could vary with the wing section,[4] so an effective angle of attack (α_{eff}) is introduced additionally for the flapping wing.[55–57] Basically, the effective angle of

Table 1. Kinematic parameters for flapping-wing motion.

Parameter	Description
Horizontal plane	Plane parallel to the ground.
Stroke plane	Plane defined by three points, as shown in Figure 1(d): wing base or root (O),wing tip at maximum ($W_{T,A}$), and minimum positions ($W_{T,B}$) based on angular measurement.
	It is near horizontal and vertical during hovering and forward flights, respectively.
Stroke angle (β)	Angle between stroke plane and horizontal plane.
	It varies from 0° (hovering) to 90° (forward).
Angle of attack (α)	Angle between wing direction and motion direction, as shown in
	Figure 1(a). Wing direction considered from trailing edge to leading edge.
Elevation angle (θ)	Angle swept by wing about z axis, as shown in Figure 1(a) and 1(c).
Flapping angle (ϕ)	Angle between leading edge and horizontal plane, as shown in Figure 1(a) and 1(b).
Torsional angle (γ)	Angle between wing direction and direction perpendicular to stroke plane.
Body angle (χ)	Angle between body line and horizontal plane, as shown in Figure 1(a).

attack depends on three factors i.e. the local flapping velocity (u_f), free stream velocity (U_∞), and prescribed angle of attack (α_u, α_d), as shown in Figure 3. According to the figure, the effective angle of attack is defined as the following equations.

$$\alpha_{eff} = \tan^{-1}\left(\frac{u_f}{u_\infty}\right) \tag{11}$$

$$\text{Downstroke} : \alpha_{eff} = \tan^{-1}\left(\frac{u_f}{u_\infty}\right) + \alpha_d - 90^\circ \tag{12}$$

$$\text{Upstroke} : \alpha_{eff} = \tan^{-1}\left(\frac{u_f}{u_\infty}\right) - \alpha_u + 90^\circ \tag{13}$$

However, the effective angle of attack may vary with the wingspan with a maximum value at the wing tip since the flapping velocity can vary along the spanwise direction.[19] If the wing flexibility is taken to account, the local flapping velocity may be affected by bending and twisting deformations. Moreover, if the flexible-wing structure behaves like a plate, plate-like deformations may result in the variations of the effective angle of attack along the chordwise direction. Therefore, the angle at the position of the three-quarter chord is likely to be used as the presentative sectional effective angle of attack.[4,55]

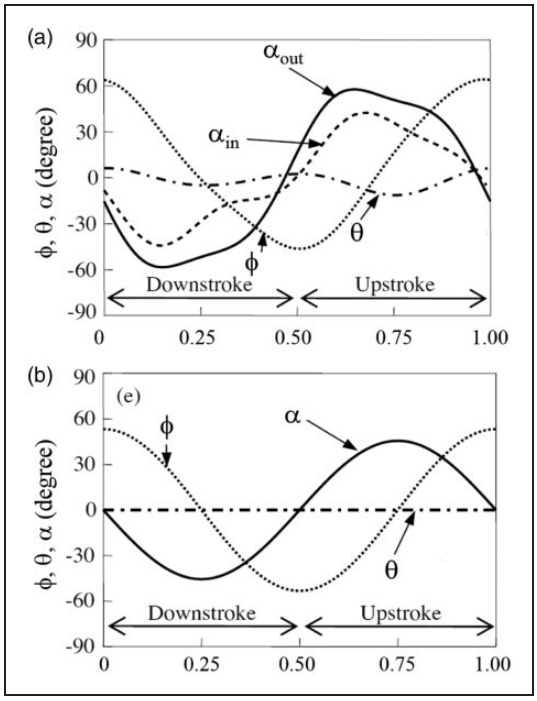

Figure 2. Variations of angle of attack (α), elevation angle (θ), and flapping angle (ϕ) for one period: (a) real wing during hovering flight of hawkmoth and (b) simplified wing using fluid-solid interaction analysis.[19]

Nondimensional numbers and parameters for flapping flight

Fundamentally, useful nondimensional numbers which are used to deal with the fluid dynamics and wing kinematics during the flight regime of biological flyers with rigid and flexible flapping wings are characterized through scaling laws. Three important nondimensional numbers are mentioned in this section.[4,58] Firstly, the Reynolds number (Re), which is the ratio of inertia forces to viscous forces in the fluid, is defined as equation (14) in the flapping-wing motion.

$$Re = \frac{\rho U_{Ref} L_{Ref}}{\mu} = \frac{U_{Ref} L_{Ref}}{\nu} \tag{14}$$

where ρ, μ, and ν are the fluid density, fluid dynamic viscosity, and fluid kinematic viscosity, respectively. U_{Ref} and L_{Ref} are the reference velocity and reference length, respectively. As well known that the flapping wings can produce both lift and thrust, the reference length is the mean wings chord length (c_m). However, the definition of the reference velocity depends upon the flight mode. Namely, in the hovering flight, it is likely to use the mean wingtip velocity (U_{tip}) as the reference velocity, so it can be expressed mathematically that $U_{Ref} = U_{tip} = 2\Phi R/T = 2\Phi fR$, where R is the length of semi span of the wing, Φ

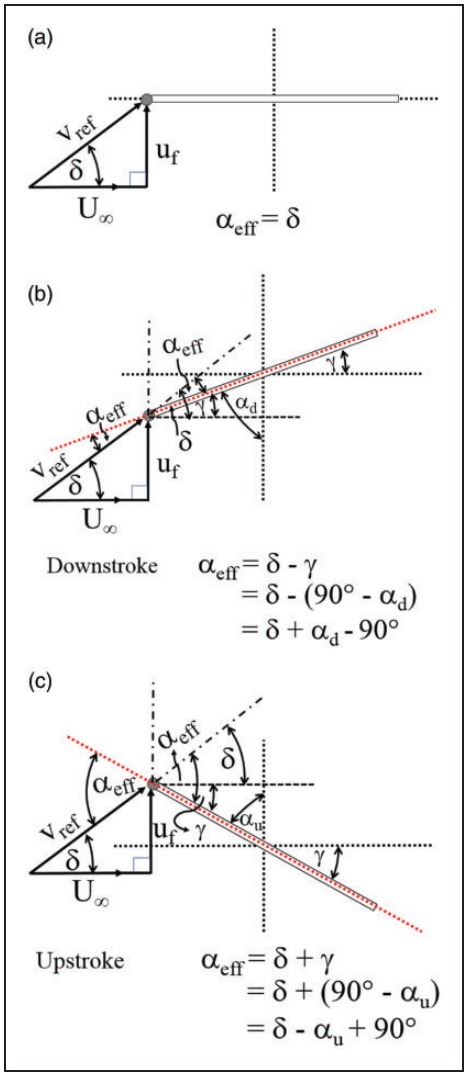

Figure 3. Effective angle of attack and its variations: (a) no vibration (b) during downstroke and (c) during upstroke.

stands for the full stroke amplitude, f is the flapping frequency, and T denotes the flapping period. Both f and T are related to the mean angular velocity (ω) as $\omega = 2\Phi/T = 2\Phi f$. Thus, the Reynolds number for 3D flapping-wing hovering flight is defined by equation (15).

$$Re = \frac{U_{Ref}L_{Ref}}{\nu} = \frac{2\Phi f R c_m}{\nu} = \frac{2\Phi R c_m}{T\nu} \tag{15}$$

If AR is the aspect ratio of the wing, which is related to the wing area (A) and wingspan (S) as $AR = S^2/A$, the wing aspect ratio can be expressed in terms of the mean wing chord and the length of the wingspan (2R), namely, $AR = (2R)^2/(2R)c_m = 2R/c_m$. Therefore, $c_m = 2R/(AR)$ and the Reynolds number may be written as equation (16).

$$Re = \frac{4\Phi R^2 f}{\nu(AR)} = \frac{4\Phi R^2}{\nu T(AR)} \tag{16}$$

For a 2D flapping wing during the hovering flight, which the forward speed is about 0, the Reynolds number is estimated by the length of the wing chord (L), the heaving amplitude (A), and the flapping frequency of the wing. Therefore, the Reynolds number is written as equation (17).

$$Re = \frac{2\pi f AL}{\nu} = \frac{2\pi AL}{\nu T} \tag{17}$$

However, during the forward flight, the Reynolds number of the flapping wing is different from that undergoing the hovering flight due to the fact that there is no forward velocity in the hovering flight. Hence, for both 2D and 3D flapping wings in the forward flight, it is possible that the reference velocity can be the forward velocity (U) or the mean velocity of the wingtip, whereas the reference length is the mean chord length. For the forward velocity, the Reynolds number is defined as equation (18).

$$Re = \frac{\rho U c_m}{\mu} = \frac{U c_m}{\nu} \tag{18}$$

Next, the Strouhal number (St), which is used to describe natural phenomena of the vortex dynamics and vortex-shedding of unsteady flow, is mentioned. For flapping flight, the St is defined as equation (19).

$$St = \frac{fL_{Ref}}{U_{Ref}} = \frac{L_{Ref}}{TU_{Ref}} \tag{19}$$

The Strouhal number depends upon the flapping frequency, the reference length, and the reference velocity. Normally, the forward velocity and the full flapping amplitude are used for the reference velocity and the reference length, respectively. Therefore, equation (19) can be written as equation (20).

$$St = \frac{fR\Phi}{U_{Ref}} = \frac{R\Phi}{TU_{Ref}} \tag{20}$$

The equation (20) is normally used to evaluate propulsive efficiency in flapping wings undergoing the forward flight.[59–62] The inverse of the Strouhal number is usually called as the advance ratio (J), which is defined as equation (21).

$$J = \frac{1}{St} = \frac{U_{Ref}}{fL_{Ref}} = \frac{TU_{Ref}}{L_{Ref}} \tag{21}$$

Finally, the reduced frequency number (k), which is used to describe the unsteady aerodynamics of pitching and heaving airfoils, is presented. The reduced frequency number is defined based on the rotational speed, the translational speed, and the mean chord length as written in equation (22).

$$k = \frac{\omega L_{Ref}}{2U_{Ref}} = \frac{2\pi f c_m}{2U_{Ref}} = \frac{\pi f c_m}{U_{Ref}} = \frac{\pi c_m}{TU_{Ref}} \tag{22}$$

In a 3D hovering flight, the mean wingtip velocity is used to calculate the reduced frequency number. Thus, the equation (22) can be modified as equation (23).

$$k = \frac{\pi f c_m}{U_{Ref}} = \frac{\pi c_m}{2\Phi f R} = \frac{\pi}{\Phi(AR)} \tag{23}$$

For a 2D hovering flight, the reference velocity is the maximum flapping velocity (2πfA). Therefore, the k is expressed as

$$k = \frac{\pi f c}{2\pi f A} = \frac{c}{2A} \tag{24}$$

However, the reference velocity is replaced with the forward velocity in the forward flight, so the k is defined as equation (25).

$$k = \frac{\pi f c_m}{U} = \frac{\pi c_m}{TU} \tag{25}$$

Since the reduced frequency number may provide a better understanding of the effect of unsteadiness of a flapping wing than the Strouhal number,[4,63] so the Strouhal number may be described in terms of the k, as expressed in equation (26).

$$k = \left(\frac{2\pi}{\Phi(AR)}\right) St \tag{26}$$

Although the Reynolds number, Strouhal number, and reduced frequency number are enough to aerodynamically characterize a rigid wing similarity, the aerodynamic performance and acoustics, as well as fluid–solid interaction caused by the effects of the wing flexibility, cannot be understood comprehensively by these dimensionless numbers. Hence, other dimensionless parameters that are involved the flexibility are introduced for aeroelastic-wing motion i.e. mass ratio (m^*), effective stiffness (S_{eff}), and effective rotational inertia (I_{eff}).[64] The mass ratio is defined as equation (27).

$$m^* = \frac{\rho_s h}{\rho_f c} \tag{27}$$

where ρ_f is the density of the air, the product of ρ_s and h denotes the surface density of the wing, and c is the characteristic length of a wing.[43] For the effective stiffness and effective rotational inertia are formed to describe the effects of the bending load and the mass moment inertia of the wing structure relative to the aerodynamic loads, respectively. The two parameters are defined as equations (28) and (29), respectively.

$$S_{eff} = \frac{E h_s^3}{12(1-\upsilon^2)\rho_f U_{Ref}^2 c_m^3} \tag{28}$$

$$I_{eff} = \frac{I}{\rho_f c_m^5} \tag{29}$$

where E denotes the elastic modulus, υ represents Poisson's ratio, h_s stands for the thickness, and I denotes the mass moment of inertia. The effective stiffness of the wing is considered like a plate stiffness which is under the elastic deflection of a bending plate.[65] Recently, it is found that the wing aspect ratio is the predominant factor determining the wing flexibility effects as well.[66] All dimensionless numbers mentioned in this section are listed in Table 2.

Governing equations of flapping flight

The flapping wings of a biological flyer under the flapping flight are governed by the Navier–Stokes equations at low speeds and if Mach number (Ma) is below 0.3, the air density is assumed to be constant because air compressibility may be ignored.[67,68] Subsequently, the airflow around flapping wings can be considered as an incompressible flow. Furthermore, if the flow is also isothermal, the air viscosity keeps unchanged. Following these consequences, the velocity and pressure (p) of the air around the flapping wing are solved through the

Table 2. Kinematic parameters for flapping-wing motion.

Dimensionless number	Description
Reynolds number (*Re*)	Defined based on L_{Ref} and U_{Ref}, air density, and viscosity. In hover, L_{Ref} is c_m, and U_{Ref} is mean wingtip velocity or flapping velocity, $U = 2\Phi R/T = 2\Phi fR$, where Φ is total flapping amplitude, R is half-span, f is frequency of flapping, and T is period of flapping.
Strouhal number (*St*)	Defined based on frequency of flapping, L_{Ref}, and U_{Ref}. It is ratio of flapping velocity to flight velocity.
Reduced frequency (*k*)	Defined based on angular velocity, L_{Ref}, and U_{Ref}. It is ratio of rotational speed to translational speed.
Advance ratio (*J*)	Defined as ratio of flight velocity to flapping velocity. It is equal to 1/Strouhal number.
Mass ratio (m^*)	Defined based on wing surface density, air density, and characteristic length of a wing.
Eff. stiffness (S_{eff})	Defined based on bending force and mass (S_{eff}) moment inertia of wing structure relative to aerodynamic forces
Eff. inertia (I_{eff})	Defined based on mass moment inertia of wing structure relative to aerodynamic forces

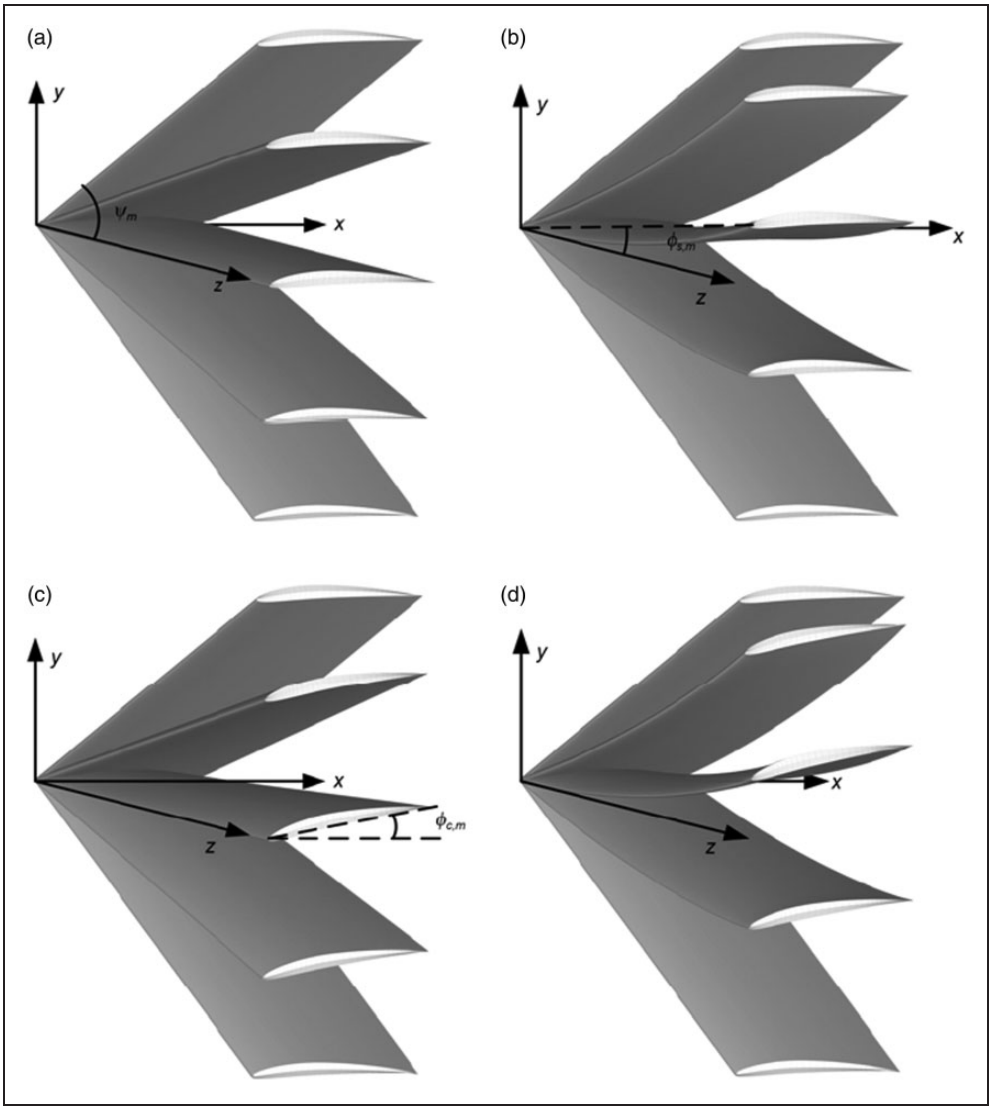

Figure 4. Schematics of flapping motion: (a) Pure rigid in single-DOF of flapping-wing; (b) spanwise deformation in down-stroke; (c) chordwise deformation in down-stroke; (d) combined spanwise and chordwise deformation in downstroke.[74]

simplified Navier–Stokes equations for an incompressible, viscous, transient, and isothermal flow, as seen in equations (30) and (31).

$$\nabla^* \cdot \mathbf{u}^* = 0 \tag{30}$$

$$\frac{k}{\pi}\frac{\partial \mathbf{u}^*}{\partial t^*} + \mathbf{u}^* \cdot \nabla^* \mathbf{u}^* = -\nabla^* p^* + \frac{1}{Re_L}\nabla^{*2}\mathbf{u}^* \tag{31}$$

Equations (30) and (31) are nondimensionalized by the reference velocity from the original forms. These equations are sufficient to a rigid flapping wing, but they are not enough to evaluate the effects of the wing flexibility. Hence, the plate-deformation equation for in-plate and out-of-plate motions is added, as seen in equation (32).[4,65]

$$S_{eff}\left(\frac{\partial^4 w^*}{\partial x^{*4}} + 2\frac{\partial^4 w^*}{\partial x^{*2}\partial y^{*2}} + \frac{\partial^4 w^*}{\partial y^{*4}}\right) = f^* + \rho^* h_s^* \left(\frac{k}{\pi}\right)^2 \frac{\partial^2 w^*}{\partial t^{*2}} \tag{32}$$

This equation is nondimensionalized from the original governing equation of the plate flapping motion.[4,69–73]

$$\frac{Eh_s^3}{12(1-\upsilon^2)}\left(\frac{\partial^4 w}{\partial x^4} + 2\frac{\partial^4 w}{\partial x^2 \partial y^2} + \frac{\partial^4 w}{\partial y^4}\right) = F + \rho_s h_s \frac{\partial^2 w}{\partial t^2} \tag{33}$$

where ρ_s is the density of the plate, F is the distributed transverse load, whereas u, v, and w are the displacement obtained in the x, y, and z directions, respectively. As illustrated in Figure 4, the characteristics of the flapping-wing motion of the rigid and flexible wings are presented.[74]

Effects on wing aerodynamic performance

In fact, biological flyers use the flapping-wing motion to generate not only lift but also thrust during their flights. This mechanism involves fluid–solid interaction which causes phenomena of vortex formation and shedding as well as the interaction of vortex dynamics and the flapping wing. Additionally, wings of the biological flyers are not rigid but flexible. The behavior of twist and bending deformation of the flapping wing changes the aerodynamic performance of the biological flyers since it affects the unsteady vortices around the wing significantly effect.[18,43] The wing deformation during flapping motion mainly depends upon aerodynamic, inertial, and elastic loads.[41] The wing flexibility leads to more complicated problems of fluid–solid interaction. Although research on the topic of aeroelasticity in the flapping-wing motion of the biological flyers has increased dynamically and rapidly for a decade, the elucidation and comprehensive understanding of aeroelastic phenomena caused by the flexibility effects are still challenging. This section reviews some recent efforts to investigate the effects of flexibility in chordwise, spanwise, and integration of chordwise and spanwise on wing aerodynamic generation and performance which is the heart of utilizing flapping-wing mechanisms for both hovering and forward flights. The recent progress in investigating the effects of flexibility on wing aerodynamic performances and characteristics is summarized in Table 3.

Chordwise flexibility

Zhao et al.[17] studied experimentally force generation of 3D aeroelastic flapping wings. They showed that the trailing-edge flexibility could be used to control aerodynamic forces and this could change the LEVs. Also, results showed that at low to medium angles of attack, the increase in the wing flexibility monotonically decreased the capability of aerodynamic-force generation but lift-to-drag ratios remained approximately constant. However, another work done by Zhao et al.[27] showed that flexible wings generated greater lift than a rigid counterpart at very high angles of attack. The systematic variations of the magnitude and direction of the net force vector and the center of pressure with wing flexibility were observed, though there were no major differences in force generation for the rigid wing and the flexible wings. Yin and Luo[43] numerically studied the wing inertia effects on the aerodynamic characteristics of 2D deformable flapping wings using an elastic plate, which might experience nonlinear deformations while flapping, during the hovering flight. They found that low mass–ratio wings provided good performance at a low frequency relative to the wing resonant frequency, whereas high mass–ratio wings provided better performance at a certain frequency close to the wing resonant frequency. Besides, the frequency ratio of 0.35 was quoted as an optimal value in their work. Their results also revealed that deformations induced by inertia and flow could enhance wing lift. However, the flow-induced deformation, which corresponded to the low-mass wing, produced low drag, thereby obtaining higher efficiency of the aerodynamic power. Dai et al.[18] further studied the investigation done by Yin and Luo.[43] They studied 3D fluid–structure interaction of flexible rectangular plates with a stiff leading edge in hovering flight at a low aspect ratio. Results showed that the wing flexibility resulted in the rate of passive pitching and the phase, thereby modifying the aerodynamics of the wing significantly. The dynamic pitching depended upon the wing stiffness, the specified kinematics at the wing root, and especially the mass ratio. They also found that an optimal frequency ratio was 0.3 approximately, which was close to the value found by Yin and Luo.[43] In general, when the frequency ratio was less than or equal to 0.3, the deformation considerably enhanced the lift and improved the lift efficiency though the wing was under the influence of a disadvantageous camber. Besides, when higher mass–ratio wings were used, the improvement in lift performance was attributed to the wing flexibility arrangement. The aerodynamic performance of a flexible airfoil under the chordwise-deformation effects was investigated by Yang et al.,[74] and the spanwise deformation angles were set as 0°, 5°, and 10° in this study. Their results showed that the large chordwise deformation angle had favorable effects: (1) the increasing of the chordwise deformation angle improved the lift and thrust characteristics; (2) when the spanwise deformation was larger, the chordwise deformation effects were stronger, as seen in Figures 5 to 7. These advantages of chordwise deformation were because the flow direction deflected backward under the deformation way. Kang et al.[75] performed the aerodynamic performance of the locally 2D flexible airfoil under unsteady viscous flow through fluid–structure interaction. Results highlighted that the fluid–structure interaction had a great impact on the lift of the elastic airfoil. Specifically, the smaller elastic stiffness increased the mean deflection of the structure, thereby inducing the mean camber effect and enhancing the lift. The frequencies affected the aerodynamic performance significantly during the unsteady scheme. Besides, it was found that when an elastic stiffness of 5×10^4 was used, when the vibrating frequencies of the airfoil had a close correlation with the shedding frequencies, the lift was improved since coherent vortices were formed. However, when an elastic stiffness of 5×10^5 was employed, the vortices formed irregularly, thereby causing the sharp drop in the lift. The results implied that an optimal frequency, which corresponded to the vortex shedding, could produce a higher lift.

Table 3. Aerodynamic performance of flapping-wing flyers summarized category of flexibility study.

Reference	Model	Fluid	Motion	Kinematics	Re/Ma/St/k/J	Aerodynamic investigation
(a) Chordwise flexibility						
[17]	3D insect-like	Oil	Hovering	Pitching	Re = 2000	Experiment: Lift–drag ratio and pressure coeff.
[18]	3D plate	Air	Hovering	Pitching	Re = 176 and 500–1000	Simulation: Lift, drag, power coeff. and lift-to-power ratio
[20]	2D plate	Air	Forward	Plunging/pitching	Re = 100	Simulation: Lift, thrust, power coeff. and thrust-, lift-to-power ratio
[21]	2D plate	Air	Hovering	Pitching/plunging	Re = 1100	Simulation: Drag, power coeff. and power-extraction efficiency
[22]	3D plate	Air	Hovering	Pitching	Re = 50–2000	Simulation: Lift, drag, power coeff. and lift-to-power ratio
[27]	3D insect-like	Oil	Hovering	Pitching	Re = 2000	Experiment: Lift-drag ratio
[30]	3D Hawkmoth-like	Air	Hovering	Pitching	Re = 400	Simulation: Lift, aerodynamic/inertial power, and pressure coeff. under isotropic flexibility
[31]	3D Hawkmoth-like	Air	Hovering	Pitching	Re = 400	Simulation: Lift, aerodynamic/inertial power and pressure coeff. under anisotropic flexibility
[43]	2D plate	Air	Hovering	Pitching	Re = 150	Simulation: Lift, drag, lift-to-drag, net/modified power and lift-to-modified-power coeff.
[74]	3D airfoil NACA4408	Air	Forward	Pitching/surging	$Re = 10^5$ Ma = 0.03	Simulation: Lift and thrust coeff.
[75]	2D airfoil NACA0012	Air	Hovering	Pitching	Re = 5000	Simulation: Lift, drag and pressure coeff.
[78]	3D airfoil NACA 0012 and plate	Water	Hovering	Plunging	Re = 16,200 and 20,250	Experiment: Thrust coeff. and thrust-to-power ratio
[79]	3D airfoil NACA0012 and plate	Water	Hovering	Plunging	Re = 9000–27,000	Experiment: Thrust coeff. and propulsive efficiency
[80]	2D airfoil NACA0014	Air	Hovering	Plunging	Re = 10,000 k = 2	Simulation: Lift, drag, input/thrust power, pressure coeff. and propulsive efficiency
[81]	3D plate	Water/air	Forward	Pitching/plunging	Re = 20,000 St = 0.2	Simulation: Thrust coeff. and propulsion efficiency
[82]	3D airfoil SG04	Air	Hovering	Pitching/plunging	$Re = 10^5$ k = 0.2	Simulation: Lift and drag coeff. and propulsive efficiency
[83]	2D plate	Air	Forward	Pitching	High Re	Simulation: Lift and propulsion coeff. and propulsive efficiency
[87]	2D airfoil NACA0015 and plate	Air	Hovering	Pitching/plunging	Re = 1100	Simulation: Lift, torque, power extraction, power consumption, net power extraction coeff. and net power extraction efficiency
(b) Spanwise flexibility						
[16]	3D airfoil NACA0012 and plate	Water	Hovering	Plunging	Re = 10,000–30,000 St = 0.05–0.9 k = 0.4–1.9	Experiment: Thrust, and power input coeff. and propulsive efficiency

(continued)

Table 3. Continued

Reference	Model	Fluid	Motion	Kinematics	Re/Ma/St/k/J	Aerodynamic investigation
[57]	3D airfoil NACA0012	Water	Hovering	Plunging	Re = 30,000 St = 0.202 k = 1.82	Simulation: Lift, thrust, and pressure coeff.
[74]	3D airfoil NACA4408	Air	Forward	Pitching/surging	Re = 10^5 Ma = 0.03	Simulation: Lift and thrust coeff.
[81]	3D plate	Water/air	Forward	Pitching/plunging	Re = 20,000 St = 0.2	Simulation: Thrust coeff. and propulsion efficiency
[88]	3D airfoil NACA0012	Water	Hovering	Plunging	Re = 30,000 k = 0.4–1.82	Simulation: Lift, thrust and pressure coeff.
(c) Combined chordwise and spanwise flexibility						
[14]	3D Hawkmoth-Manduca sexta-like	Air	Hovering/forward		Re = 10,000	Simulation: Lift force and coeff. and mechanical power
[15]	3D plate	Air	Forward		Re = 10,000 J = 0.5	Simulation: Lift, thrust, power coeff. and propulsive efficiency
[19]	3D Hawkmoth-Agrius convolvuli-like	Air	Hovering	Reciprocating/ pitching	Re = 6300 k = 0.3	Simulation: Vertical and horizontal forces, aerodynamic power and efficiency, and induced power
[24]	3D FruitFly-like	Air	Hovering		Re = 150	Simulation: Lift, and drag coeff. lift-to-drag, lift-to-power ratios and power consumption
[25]	3D TL-Flowerfly-like	Air	Hovering		Re = 5000	Simulation: Lift, drag, and input power coeff. and efficiency
[26]	3D Bumblebee-like	Air	Hovering/forward		Re = 2280 J = 0.22	Simulation: Lift, thrust, input power coeff., efficiency and power economy
[28]	3D Hawkmoth-Manduca sexta-like	Air		Pitching/rolling		Simulation: Power reduction
[29]	3D membrane	Air	Hovering/forward		Re = 4342–13,025 J = 0, 0.25, 0.5	Simulation: Thrust
[33]	3D membrane	Air	Hovering	Pitching	Re = 7,800	Simulation: Lift coeff. and normal force
[66]	3D plate	Water	Hovering	Pitching	Re = 5,300	Experiment: Lift and drag coeff. and total force
[74]	3D airfoil NACA4408	Air	Forward	Pitching/surging	Re = 100,000 Ma = 0.03	Simulation: Lift and thrust coeff.
[89]	3D plate	Air	Forward		Re = 10,000–100,000 J = 0.3–8	Experiment: Lift and thrust coeff.
[90]	3D Hummingbird-like	Air	Forward		Re = 2500, 3500, and 4700 k = 0.46, 0.49, 0.62, and 0.93	Experiment/Simulation: Lift and drag
[91]	2D Bumblebee-like	Air	Hovering/forward		Re = 157 J = 0 and 0.12	Simulation: Aerodynamic forces and power
[93]	3D Hawkmoth-Manduca sexta-like	Air	Hovering	Pitching	Re = 7027	Experiment: Lift and thrust
[94]	3D Hummingbird-like	Air	Hovering	Reciprocating	Re = 1500–12,200	Experiment: Thrust
[96]	3D DelFly-like	Air	Hovering/forward	Claping/flinging	Re = 20,000. k = 1	Simulation: Thrust and pressure coeff.
[97]	3D FlowerFly-like	Air	Hovering	Claping/flinging	Re = 16,000	Experiment/Simulation: Lift and pressure
[98]	3D membrain	Air	Forward	Reciprocating	k = 0.7–4	Experiment: Thrust coeff. and propulsive efficiency
[99]	3D membrane	Air	Forward		–	Experiment: Lift and thrust

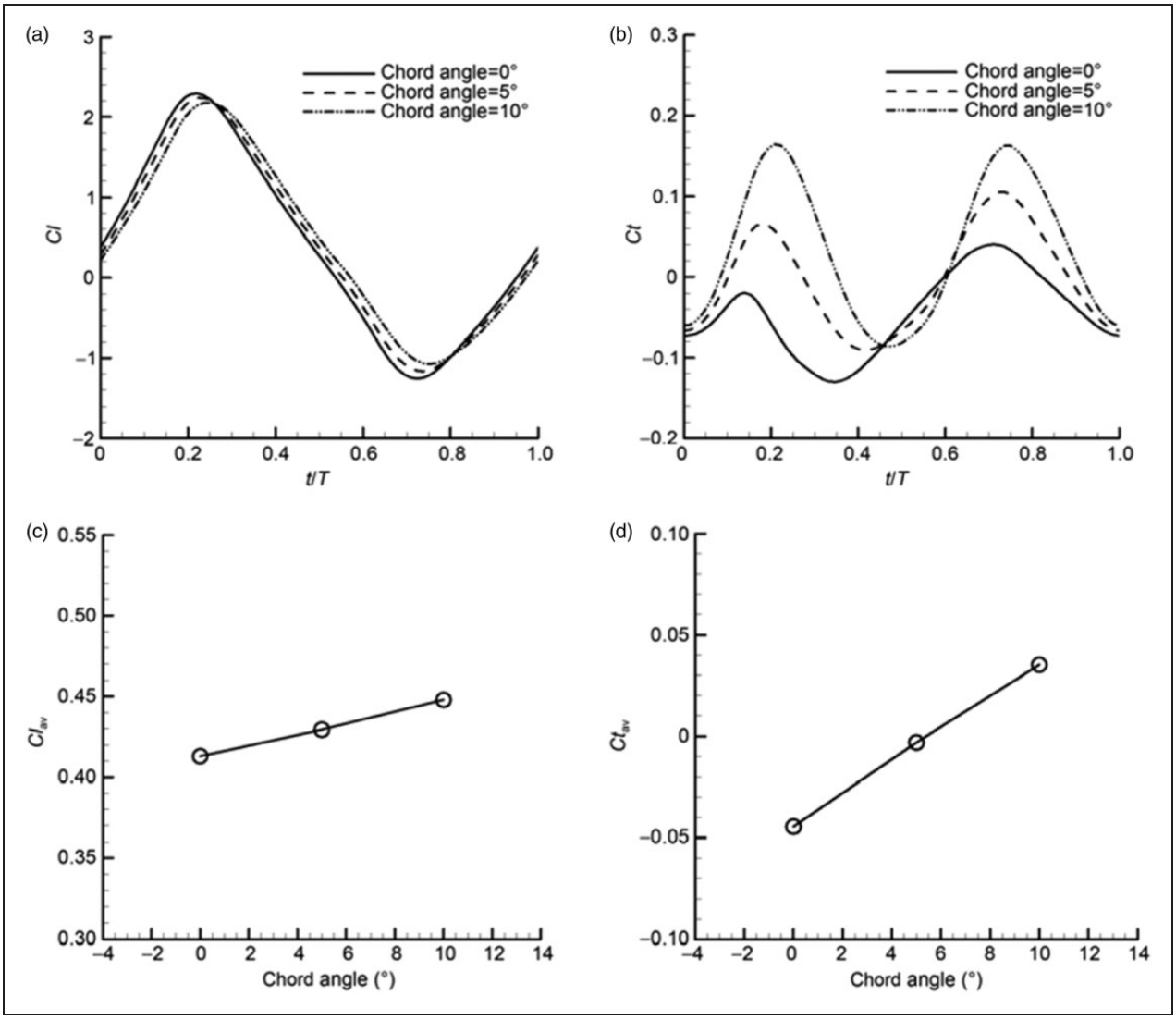

Figure 5. Chordwise deformation effects when spanwise deformation angle was 0°. (a) Lift coefficient; (b) thrust coefficient; (c) average lift coefficient; and (d) average thrust coefficient.[74]

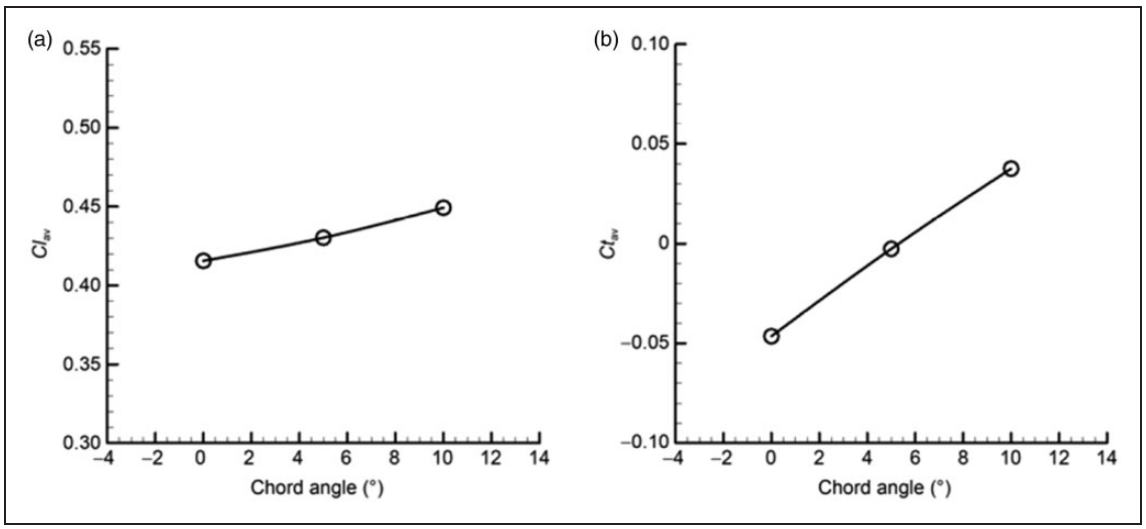

Figure 6. Chordwise deformation effects when spanwise deformation angle was 5°. (a) Average lift coefficient and (b) average thrust coefficient.[74]

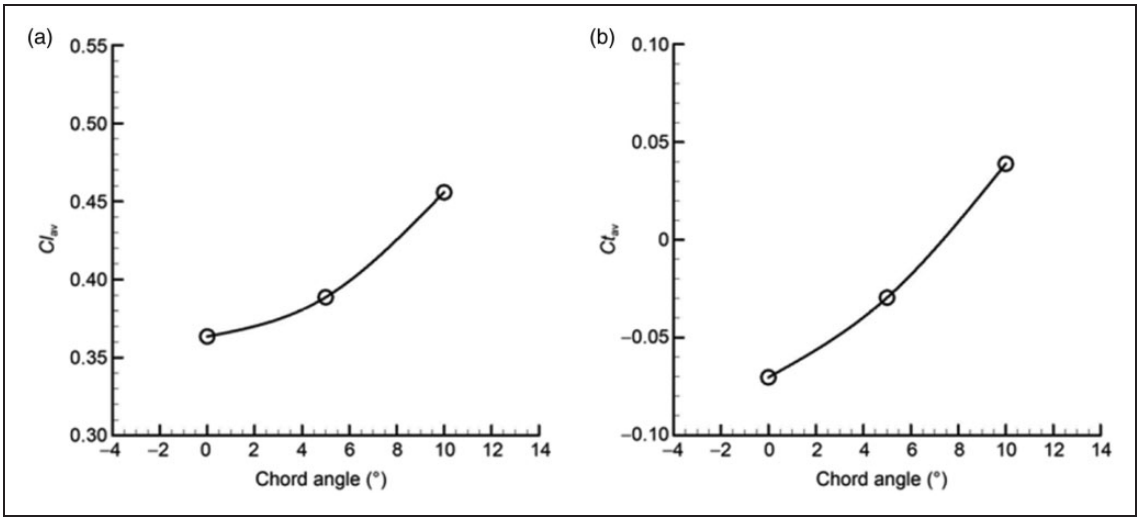

Figure 7. Chordwise deformation effects when spanwise deformation angle was 10°. (a) Average lift coefficient and (b) average thrust coefficient.[74]

Cheng and Lan[22] drew the conclusion obtained from a study of the aerodynamic performance of a 3D flapping wing under the chordwise-flexibility effects during the hovering flight using a rectangular flat plate. It was found that generally, the lift performance could be reduced by the wing flexibility since the LEV structure of the flexible wing was smaller than that of the rigid one. Moreover, with the significant difference in TEV structures between the rigid and flexible wings, the TEVs of the flexible wing were not formed yet, whereas the TEVs of the rigid wing were detached and shed from the wing. As a result, vortex structures were changed, as seen in Figure 8 which showed the vortices at three instant times during early downstroke. For the flexible wing, the large negative camber seriously suppressed the formation of TEV, thereby leading to a reduction in the LEV strength. Following this, lower lift was found during the consequence of the flapping motion because the rate of change of fluid impulse was lower. However, in the early downstroke of the rigid wing, a ring-shape vortex, which was an integration of LEV, TV, and TEV, was formed because of translational acceleration and pitch rotation. As the wing motion continued, the LEV still attached to the top surface of the wing, whereas the TEV detached and shed from the wing. With these phenomena, the rate of change of fluid impulse became larger, then high aerodynamic forces were produced.[76] However, it was found that when pitch rotation was delayed or stroke amplitude was low, the flexible wings generated more lift when compared to rigid counterparts. Moreover, the lower power consumption was obtained by the flexible wings and the improvement in the lift performance of the very flexible wings could be done effectively by reducing the stroke amplitude.

Normally, most insect wings are flexible and it seems that the wings get deformable under the combined loads of their inertia and aerodynamic forces in nature.[20,43,77] Tian et al.[20] numerically studied lift and thrust production of an elastic wing under the effect of wing flexibility in forward flight by means of 2D simulation of fluid–structure interaction. The wing was prescribed by pitching around the leading ledge and translating in an inclined stroke plane. Also, the effects of mass ratio, stroke angle, and flight speed on the aerodynamic force generation were mentioned. Results showed that the significant increase in thrust was done by the passive pitching due to the wing deformation and it was possible that lift was maintained or increased in this situation. Another important result was mentioned that a larger magnitude of the chordwise deformation was found during upstroke than downstroke, though actuation kinematics and the wing structure were symmetric. This agreed with the conclusion drawn by Luo et al.[77] In addition, the role of the fluid-induced deformation and the asymmetry deformation was underlined when the mass ratio of the flexible wing was low. Shahzad et al.[31] studied the aerodynamic characteristics of deformable-flapping wings, which had different aspect ratios, i.e. $AR = 1.5$, 2.96, 4.5, and 6.0, and wing shapes, i.e. $r_1 = 0.43$, 0.53, and 0.63, in hovering flight at $Re = 400$. The flexibility of the wings was homogeneous and isotropic. The radius of the first wing-area moment was represented as the wing shape. Their results indicated the degree of flexibility resulted in pitch angle kinematics, thereby altering aerodynamic forces in terms of lift, power including magnitudes of lift and power peaks. Besides, the mass ratio as well as the wing shape also affected lift and power. Lower lift generated by flexible wings with high AR of 4.5 and 6.0 was observed when compared to the rigid counterpart for mass ratios of 0.66 and 4 since pitch angles were lower during the mid-stroke, as seen in Figure 9. However, the power economy (PE) of the flexible wings was higher than that of the rigid wing, as seen in Figure 10.

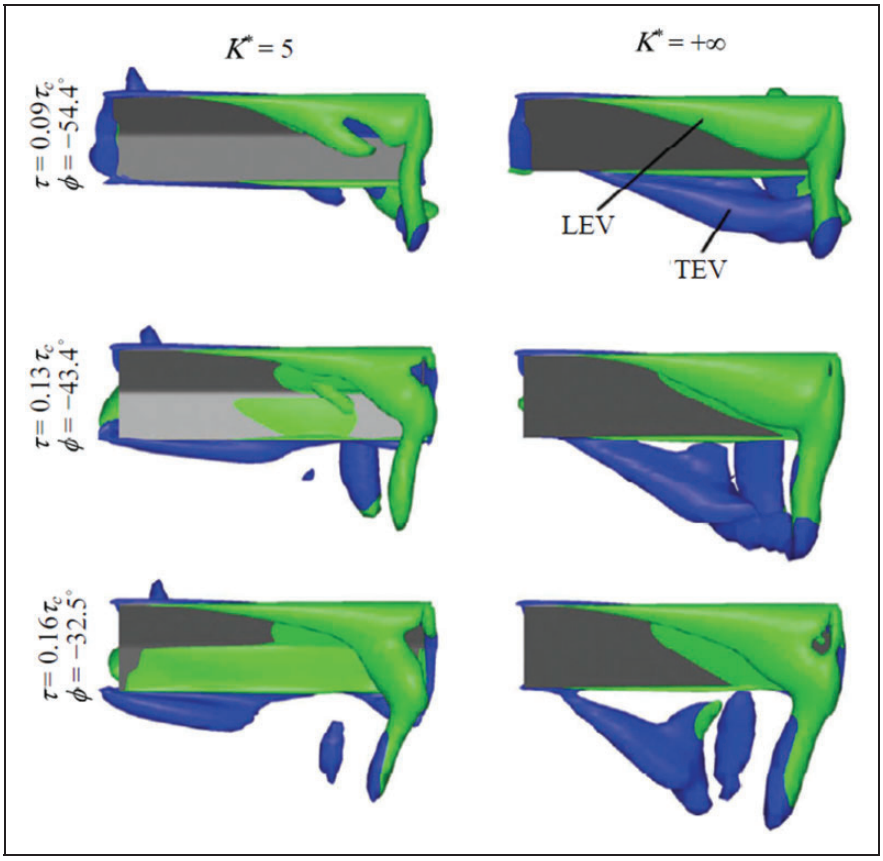

Figure 8. Iso-surface plots of flow and vortex structures during early downstroke ($\tau = 0.09\tau_c$ to $0.16\tau_c$) for flexible wing ($K^* = 5$) and rigid wing ($K^* = \infty$) using $Q = 5$: green was negative and blue was positive.[22]

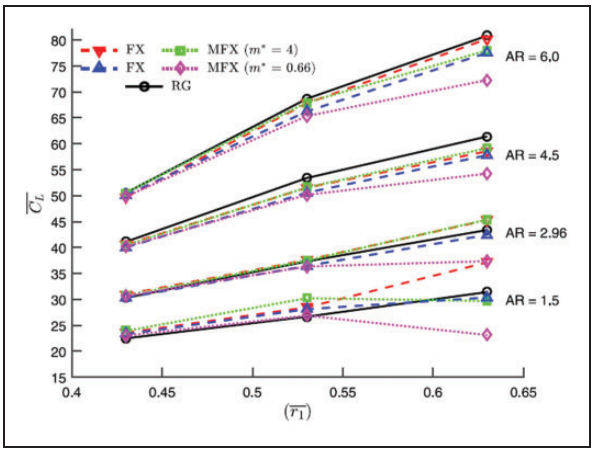

Figure 9. Correlation between lift coefficient (C_L) and wing shape (r_1) at AR = 1.5, 2.96, 4.5, and 6.0 with mass ratio (m^*) = 4.0, and 0.66. RG, FX, and MFX were rigid, flexible, and more flexible wings, respectively.[31]

In an extended study done by Shahzad et al.,[30] they studied the wing flexibility, which was anisotropic, on the aerodynamic performance of hawkmoth-like flapping wings. The mechanisms, which were related to the aerodynamic characteristics of these wings, were compared at AR = 1.5 and 6.0, as illustrated in Figure 11. At AR = 1.5, it highlighted the domination of the chordwise deformation caused by the anisotropic flexible structure of the wings. Subsequently, it could affect lift generation at different phases of the cycle, whereas at high AR = 6.0, the wings also had dominant spanwise deformation. Also, the combined deformation in the chordwise–spanwise direction affected lift production at different phases of the cycle. In addition, their results indicated that the mean lift was increased by flexibility as much as 39%, 18%, and 17.6% at AR = 1.5, 2.96, and 4.5, respectively, for all wing shapes. Nonetheless, flexible wings gave lower lift than the rigid wings at AR = 6.0, and the $r_1 = 0.53$ and 0.63, as seen in Figure 12. This was because small positive lift or negative lift was observed before the stroke. They also pointed out that the trends in Figure 13 indicated that when AR and r_1 decreased, C_L typically decreased but PE increased, especially the wings with AR = 2.96 and 4.5, and $r_1 = 0.43$ and 0.53. The C_L also decreased as the wing area increased. However, the power efficiency might be uncertain when considering overall under the anisotropic flexibility in hovering flight, and it was possible that these results were different for other flight modes.

Heathcote et al.[78] studied thrust generation for a 2D airfoil plunging at zero freestream velocity under the effect of airfoil stiffness in a water tank. They found that the airfoil with the least stiffness could

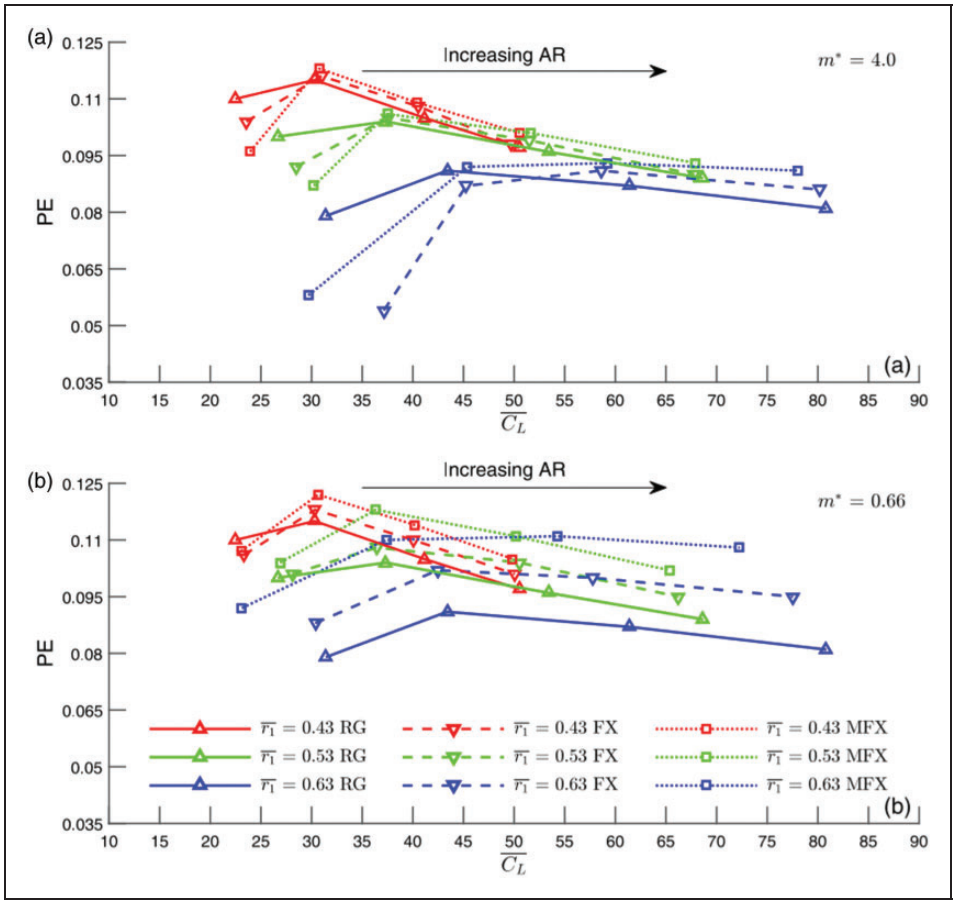

Figure 10. Correlation between power economy (PE) and lift coefficient (C_L) for different ARs and wing shapes (r_1) when mass ratio (m^*) (a) = 4.0 and (b) = 0.66. RG, FX, and MFX were rigid, flexible, and more flexible wings, respectively.[31]

generate larger thrust at low frequencies, whereas the thrust coefficient of the intermediate stiff airfoil was greatest at high frequencies in plunging motion. Also, the thrust/input-power ratio of the flexible airfoils was greater than that of the rigid airfoil. They also indicated that apart from plunge frequency and the phase lag and amplitude of the trailing edge, the airfoil flexibility had a great influence on alternating vortex streets or vortex pairs, thereby causing thrust generation. Heathcote and Gursul[79] experimented with chordwise-flexible airfoils heaving with constant amplitude for Reynolds numbers of 9000–27,000 in the water tunnel. They found that a degree of flexibility increased propulsive efficiency and thrust coefficient. Moreover, it was found that the chordwise flexibility could provide positive effects for airfoils under purely heaving motion at low Reynolds numbers. Their measurements revealed weaker LEV corresponding to higher propulsive efficiencies and stronger TEV corresponding to higher thrust coefficients. Besides, propulsive efficiency and thrust coefficient were functions of the pitch phase angle and Strouhal number. The peaks of thrust coefficient were found at pitch phase angles in the region of $110-120^\circ$ but at higher Strouhal numbers. The peaks of propulsive efficiency were found at a Strouhal number of 0.29 and a pitch phase angle of $95-100^\circ$, which matched the range observed in nature. Miao and Ho[80] investigated the influence of flexibility and chordwise amplitude on aerodynamic characteristics of a flapping airfoil at Reynolds number of 10^4 and reduced frequency of 2 during plunge motion. Their results revealed the formation of a pair of LEV along the flexible airfoil as it underwent the plunge motion. The formation of thrust-indicative wake structures was found when the flexure amplitude of the airfoil was less than 0.5 of the chord length. When flexure amplitude was 0.3 of the chord length, the propulsive efficiency of the flapping airfoil was enhanced. The results also indicated a correlation between the reduced frequency and propulsive efficiency. The highest propulsive efficiency was found at the Strouhal number of 0.255. Zhu[81] numerically investigated the aerodynamic performance of a foil immersed in air and water under the effect of structural deformation at different amplitudes of pitch (θ_0). Their results showed that the aerodynamic performance of the foil in the water and air was caused by the change of the effective pitch angle and the effective angle of attack. These results corresponded to the conclusion drawn by Heathcote et al.[78] In the water, the propulsion efficiency increased as large as 20%, but thrust decreased as Young's modulus was reduced. However, both the thrust and the efficiency

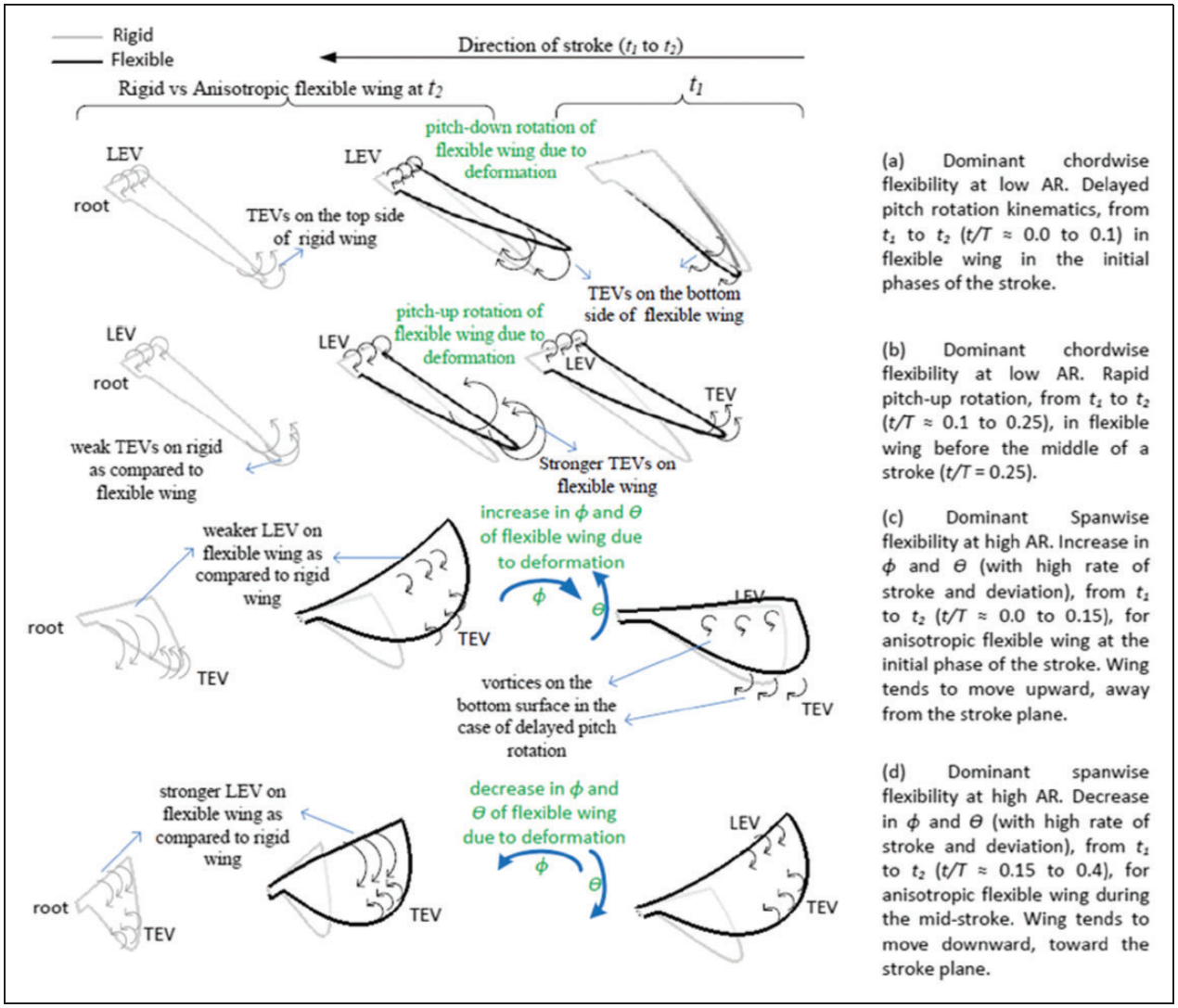

Figure 11. Schematic diagram of anisotropic-flexible-wing mechanisms. Vortex size represented its strength. Time of flapping motion was from t_1 to t_2. Light lines were rigid wings and dark lines were flexible wings.[30]

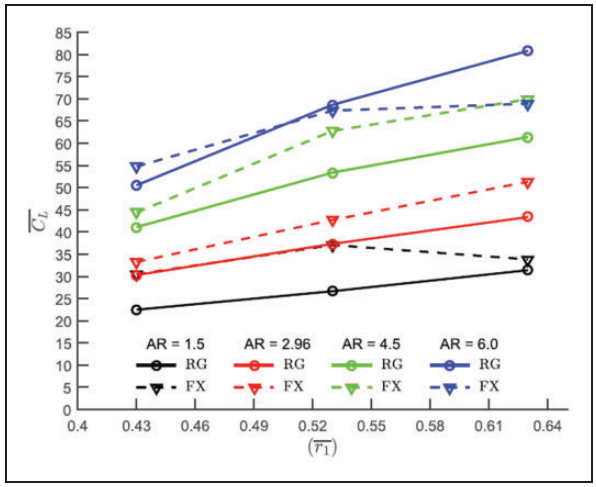

Figure 12. Correlation between C_L and wing shapes at different ARs. RG and FX were rigid and flexible, respectively.[30]

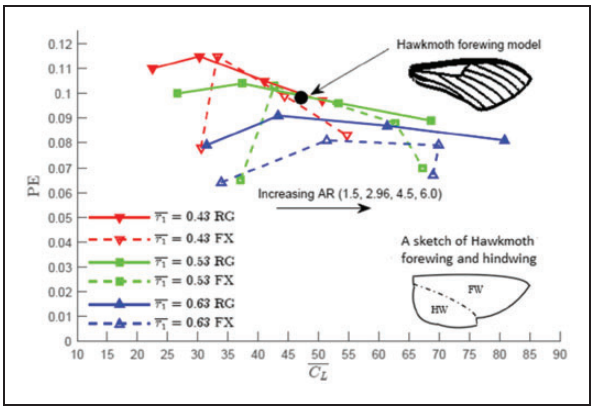

Figure 13. Correlation between PE and C_L at different wing shapes and ARs. RG and FX were rigid and flexible wings, respectively. HW and FW were for hindwing and forewing in the sketch of the hawkmoth wing.[30]

plunged in the air when Young's modulus reduced. This stressed the importance of chordwise flexibility to propulsion efficiency improvement. Unger et al.[82] studied the improvement of the propulsive efficiency of a flexible flapping airfoil at low Re conditions. They found that propulsive efficiency was reduced when more degrees of flexible were employed for the airfoil. However, an improvement in the efficiency could be obtained by more stiffness during the downstroke and more flexibility during the upstroke. Ulrich and Peters[83] presented a 2D flexible airfoil performing sinusoidal deformations at high Reynolds numbers in terms of propulsive force, lift force, generalized pitching, and bending forces. These forces were found as functions of reduced frequency number, nondimensional wavelength, and amplitude. Their results showed that when the moving speed was lower than the wave speed, a positive propulsive force generated by the sinusoidal deformations existed. When the moving speed was equal to the wave speed, the system was under all zero forces. When the moving speed was greater than the wave speed, the energy was extracted. Tian et al.[21] further studied power extraction from rigid airfoil wings under the effects of flexibility done by the references.[84–86] Results of Tian et al.[21] indicated that the power-extraction efficiency was enhanced by flexible airfoils. Also, they investigated the power-extraction capability of flapping plates under the effects of flexibility, including active control. Their results showed that with the certain kinematic parameters, the flexibility could not improve the capability of power extraction of the flexible plate significantly, whereas the rigid plate with the active control on the leading segment increased the power coefficient by 11.3%, as seen in Figure 14. Their results also revealed that most power-coefficient increments were caused by the presence of vortex and distributions of pressure near the plate, including the projection plate area in the translational direction. Wu et al.[87] numerically investigated the improvement of power extraction of a 2D NACA0015 airfoil with a flexible tail. The airfoil was forced in pitching and induced plunging motions under a laminar flow with Reynold number of 1100. The power was extracted by a rigid or deformable flat plate attached to the trailing edge of the airfoil. Their results indicated that the flexible tail of the airfoil provided more efficiency of net power extraction than for the rigid tail. Besides, they found that the increased lift force enhanced power extraction and the increased power extraction directly improved to net efficiency. Moreover, a highly flexible tail performed high enhancement of power extraction.

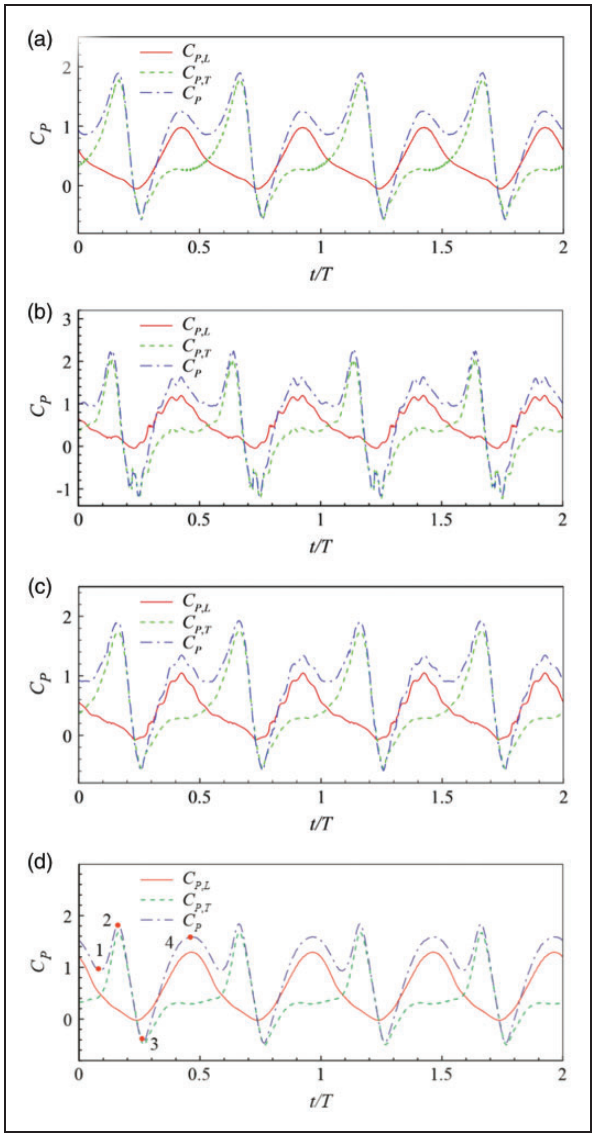

Figure 14. Performance of (a) rigid plate, (b) flexible plate, (c) plate with flexible leading part and rigid trailing part, and (d) rigid plate with active control for two periods of $C_{P,L}$, $C_{P,T}$, and C_P.[21]

Spanwise flexibility

Zhu[81] also investigated the efficiency and thrust of a flapping foil under the effects of the spanwise direction in water and air. Results indicated that in water, the thrust produced by the rigid foil is much higher than that by the flexible one. However, there was no significant difference in propulsion efficiency when flexure changed. For the study in the air, if the stiffness of the foil was ranged from 10^4 to 10^5, the efficiency was changed slightly and the thrust dramatically increased with the flexibility as much as nearly 100% thrust gain. Besides, the results showed the important role of heaving amplitude along the spanwise direction of the foil to thrust and efficiency. Namely, the depletion of thrust in water was due to the decrease in heaving amplitude, thereby reducing both the energy input and thrust generation. Subsequently, the efficiency kept unchanged, while the thrust increment in the air was the consequence of the increment of heaving amplitude. Heathcote et al.[16] experimentally studied the thrust, power–

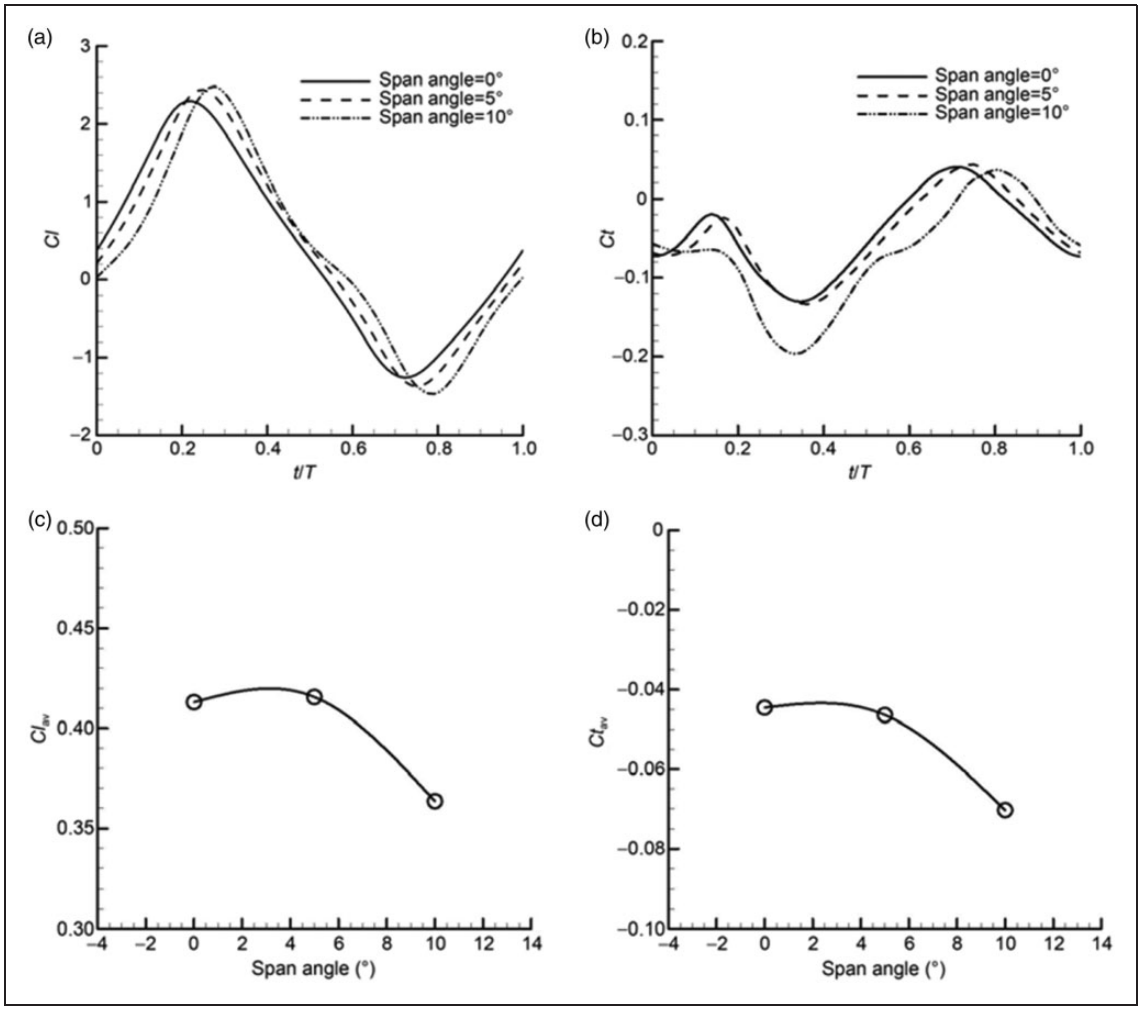

Figure 15. Spanwise deformation effects when chordwise deformation angle was 0°. (a) Lift coefficient; (b) thrust coefficient; (c) average lift coefficient; and (d) average thrust coefficient.[74]

input, and propulsive efficiency of a rectangular wing under the effect of spanwise flexibility. The wing with an aspect ratio of 6 and heaving oscillation at one end was tested in water at Reynold numbers from 10,000 to 30,000. Three wings with changeable spanwise stiffness and rigid in the chordwise direction were tested. They found that a wing with intermediate flexibility contributed to a 50% thrust benefit. Nonetheless, a reduced thrust coefficient was found for a highly flexible wing. In addition, excessive spanwise flexibility caused large tip phase lags between root and tip. Then, the opposite couple–vorticity formed near the root and the tip, causing a weak vorticity pattern. Following these phenomena, thrust coefficients decreased significantly. Several important conclusions obtained from Chimakurthi et al.[88] indicated that (1) within the studied range of dimensionless parameters, a favorable effect on the thrust generation was provided by spanwise flexibility. (2) Leading-edge suction was an important factor, which could affect thrust generation, during the plunging motion of the leading-edge–curvature wings. (3) Within the range of reduced frequency numbers from 0.4 to 1.82, the increase in the reduced frequency number resulted in the increment of thrust generated by flexible and rigid wings. Aono et al.[57] numerically investigated flapping wing aerodynamics under the influence of spanwise flexibility using a rectangular wing, which had an aspect ratio of 3 and an NACA 0012 airfoil cross section, undergoing pure plunge at Reynolds number of 3×10^4 and reduced frequency number of 1.82. They concluded that wing deformation could enhance mean and instantaneous thrust forces within a suitable range of spanwise flexibility. Also, additional conclusions were drawn. Namely, phase lag of the wing tip played a key factor for thrust generation. For example, when the phase lag was less than 90°, spanwise flexibility provided a favorable effect on the thrust generation. The effects of the spanwise flexibility on wing lift were also investigated by Yang et al.[74] for a flexible airfoil when the chordwise deformation angles were set at 0°, 5°, and 10°, respectively. They indicated that when the chordwise deformation angle was small, the larger spanwise deformation could lead to the worse lift and thrust characteristics, as shown in Figures 15 and 16.

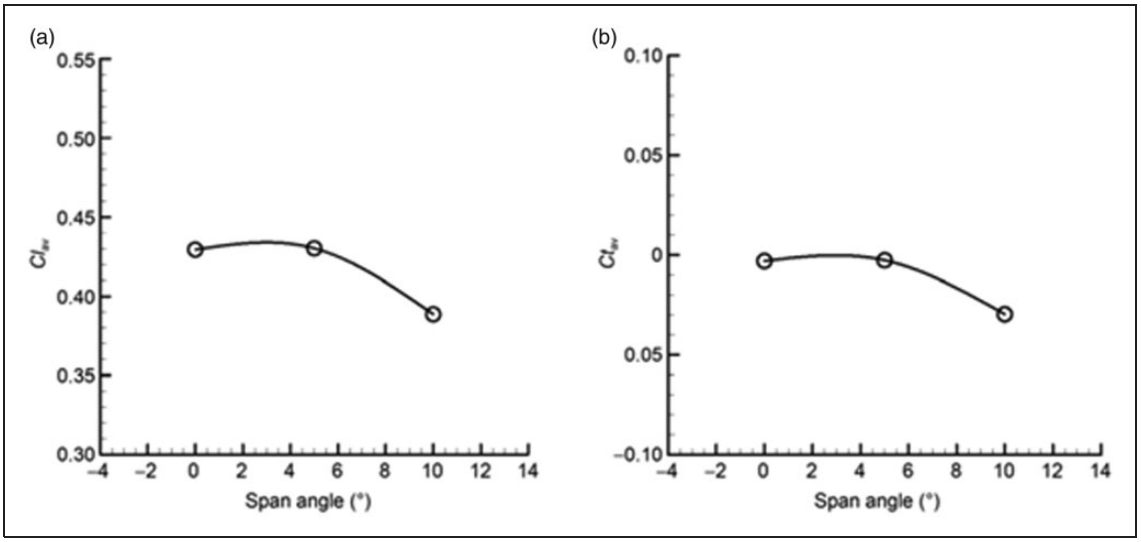

Figure 16. Spanwise deformation effects when chordwise deformation angle was 5°. (a) Average lift coefficient and (b) average thrust coefficient.[74]

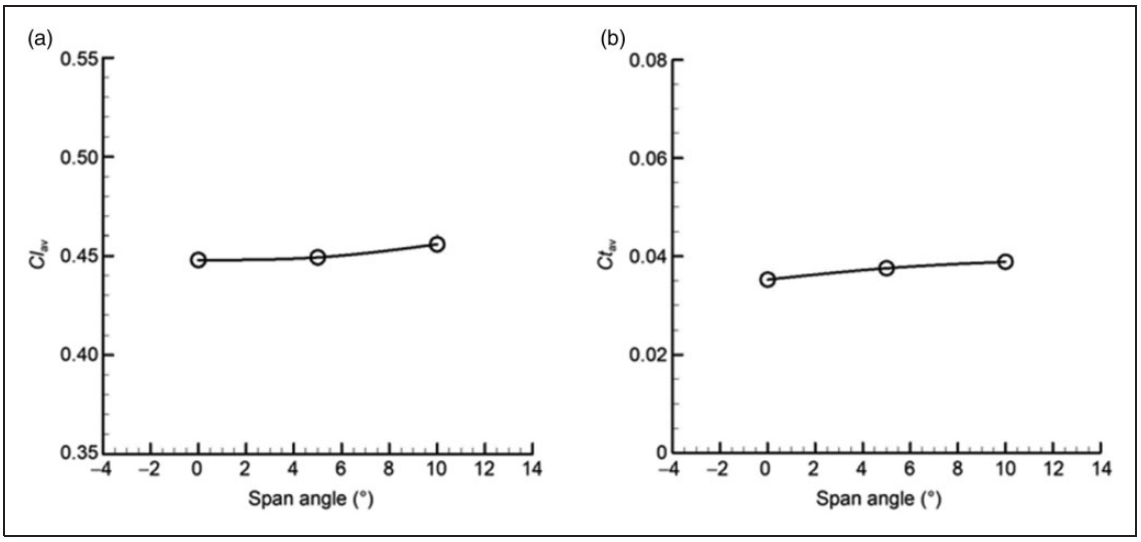

Figure 17. Spanwise deformation effects when chordwise deformation angle was 10°. (a) Average lift coefficient and (b) average thrust coefficient.[74]

When the chordwise deformation angle was large, the large spanwise deformation could improve the lift and thrust characteristics slightly as shown in Figure 17. These phenomena indicated that (1) when the chordwise deformation was large, the spanwise deformation might also be larger and (2) the spanwise deformation should be less than the chordwise deformation.

Combined chordwise and spanwise flexibility

The effects of combined chordwise and spanwise flexibility on the aerodynamic performances have been highlighted by several researchers. Gopalakrishnan and Tafti[15] numerically studied these effects on the lift and thrust production in flapping flight using an elastic membrane, which was under the in-plane prestress condition, during forward flight with an advance ratio of 0.5 and at Reynold numbers of 10,000. The role of prestresses was presented to the suitable camber and the aerodynamic pressure. Results showed that the camber given by the flexible wing increased the generation of thrust and lift significantly. For flexible wings, the LEV kept attached on the top surface and moved along with the camber and could cover a major part of the wing, thereby resulting in high force generation. For rigid wings, the LEV detached from the surface, thereby causing lower force generation. Furthermore, the given camber increased the force component, which contributed to thrust. This led to a high thrust-to-lift ratio. Hu et al.[89] carried out an experimental study of the aerodynamic performances of rigid, flexible, and very flexible wings undergoing flapping flight. They indicated different performances obtained by flapping flight

and fixed-wing soaring flight. Results revealed that the wing–skin flexibility had significant effects on aerodynamic performances for both flights. The flexible and very flexible wings provided a better lift-to-drag ratio than the rigid counterpart during soaring flight. This situation was noticeable when the soaring speed was high or the angle of attack was relatively high. Nonetheless, for flapping flight, the rigid wing generally gave better performance of lift production than the two flexible wings. Also, the results indicated that overall, the flexible wing had the best aerodynamic performance during the soaring flight but it performed the worst aerodynamic performance in flapping flight, whereas the very flexible wing generated the best performance in terms of thrust during flapping flight. Nakata et al.[90] computationally and experimentally evaluated aerodynamics of a four-flexible-wing hummingbird during the clap and fling.

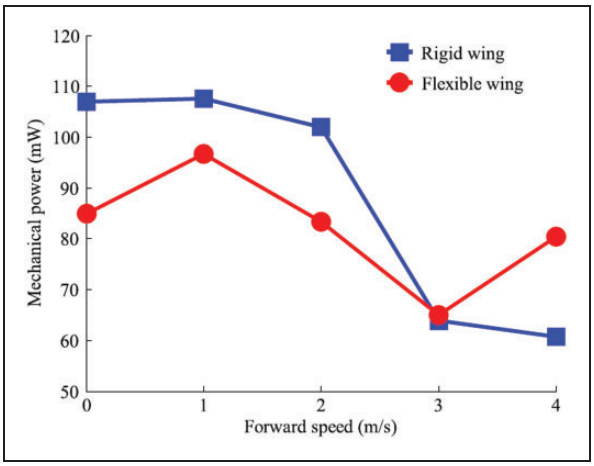

Figure 18. Comparison of mean-mechanical power at different speeds of rigid and flexible MAVs.[14]

They deemed that the adjustment of the angle of attack near the wing tip at stroke reversal could avoid the delay of some unfavorable phase during wing rotation. Following this phenomenon, force production was increased. Yang et al.[74] carried out the combined effects of chordwise and spanwise flexible on the aerodynamic performance of the airfoil in flapping flight. They concluded that the performance in terms of aerodynamic forces of micro-sized wings could be improved and degenerated due to large chordwise and large spanwise deflections of the wing, respectively. They suggested that the chordwise deformation should increase to 25° at a 5° spanwise deformation angle so that the chordwise deformation angle could enhance aerodynamic performance in a certain range. Nguyen et al.[24] modeled and analyzed flexible wings of a fruit fly for the aerodynamic evaluation at Reynolds number of 150. Their results indicated that the leading-edge-reinforced (LER) wings, which the stiffness decreased sharply in spanwise and chordwise directions, performed deformation well like insect wings during flight and could provide significantly better ratios of lift-to-drag and lift-to-power than the uniform flexible and rigid wings. Nguyen and Han[14] explored the effects of the anisotropic structure of a hawkmoth Manduca Sexta flexible wing on several characteristics of flight. They indicated that it needed more mechanical power consumption at a low speed, as seen in Figure 18, due to the more demand for lift generation in hovering flight and at low forward speed, which the stroke angle is nearly 0°, thereby causing the almost vertically downward induced flow and a source lift generation as seen in Figure 19(a). Moreover, the benefit of downward flow and the mechanism of lift production could be contributed by wing deformations due to the swift stroke reversal motion.[19] Therefore, the utilization

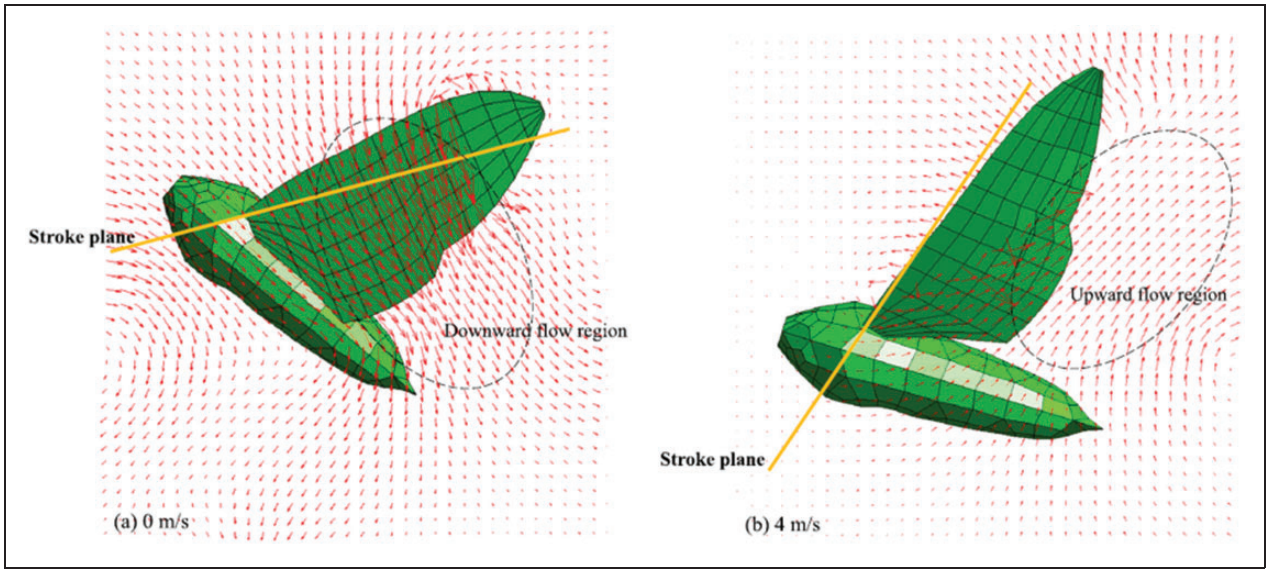

Figure 19. Comparison of flow fields at different forward speeds (a) 0.0 and (b) 4.0 m/s; shown at beginning of downstroke.[14]

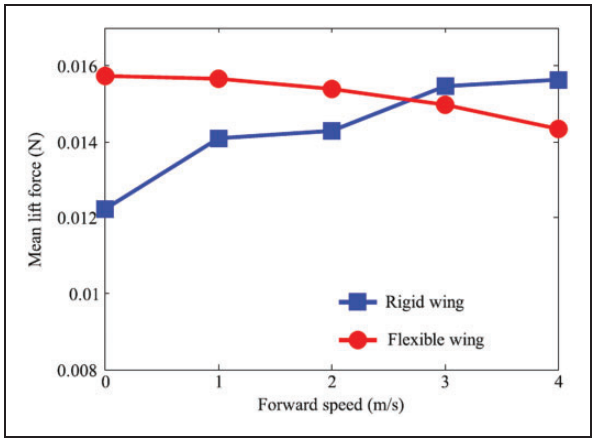

Figure 20. Comparison of mean lift generated by rigid and flexible MAVs at different forward speeds.[14]

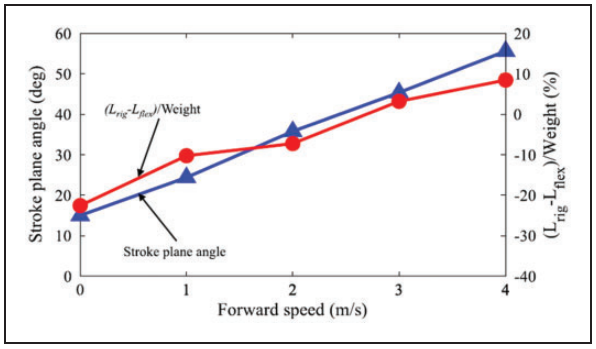

Figure 21. Stroke angle (β) and difference of lift generated by rigid and flexible MAVs at different forward speeds.[14]

of flexible wings had high efficiency at low speeds. They also indicated 20.6%, 10.3%, and 18.6% reductions of the mean mechanical power at forward speeds of 0.0, 1.0, and 2.0 m/s, respectively. However, the direction control of the resultant force was needed at a higher speed, so the stroke angle was increased passively by the wing. Besides, the detriment of the lift generation mechanism at 4.0 m/s was found because the stroke plane was almost vertical due to the appearance of the upward flow region at the start of the downstroke, as shown in Figure 19(b). As a result, this upward flow region was intensified by the influence of wing deformations, thereby reducing the lift force. To avoid this situation, the flexible wing had to increase the flapping frequency for sufficient lift production. Consequently, at 4.0 m/s, the required flapping frequency of the flexible wing was higher than that of the rigid wing, namely, it was 1.12 times approximately. At the same speed, the total mechanical power of the flexible wing was increased to 1.4 times that of the rigid wing, as indicated in Figure 18. This result seemed to correspond to the previous study done by the open literature.[49] Namely, the major parts of mechanical power were proportional to frequency cubic during high-speed flight. Besides, a comparison of mean lift generated by the rigid and flexible wings under the steady-state conditions of the flexible wing was depicted in Figure 20. When the wing underwent hovering or flying condition at low forward speeds, the mean lift produced by the flexible wing was higher than that by the rigid one. Nonetheless, this effect was reversed during high-speed flight. Their results also indicated the correlation of the forward speed, the lift difference between the rigid and flexible wings, and the stroke angle due to the direction of the flow induced by wing deformations, as seen in Figure 21. When stroke plane was small, this flow was nearly vertical, causing the lift enhancement. However, when the stroke plane increased, this enhancement became less noticeable.

Tobing et al.[26] further investigated the flexibility effects on wing propulsion from an earlier study done by Lu et al.,[91] which used a 2D bumblebee wing model, using a 3D bumblebee wing model. Results indicated that the lift force of the 3D flexible wing was around 30% higher than that of the rigid one because the twist and bending deformations of a flexible wing balanced the pressures on its surfaces. This caused a longer time and more stability of LEV attachment on the flexible wing than the rigid wing. This suggested that the flexibility played an important role in preventing LEV separation and then improving the lift generation of flapping insect wings, which was supported by an earlier observation done by Mountcastle and Combes[92] as well. Tay[25] numerically investigated the aerodynamic performance of a 3D flapping wing of TL-Flowerfly-micro flyer with two- to six-wing flapping configurations under the effects of flexibility as well as kinematic motions. Results showed that a flexible chordwise and rigid spanwise wing produced the highest lift with the minimum power. The lift produced by each wing of the two-, four-, six-wing configurations was different slightly. They concluded that although a higher total lift force could be generated by more wings, it required higher drag and power. Another experimental study of the flexibility effects on the aerodynamic performance of flapping wings was conducted by Fu et al.[66] This experiment was done at an angle of attack of 45° and Reynolds number of 5.3×10^3 (based on the chord length and the wing tip velocity). Their results indicated that deformable wings with an aspect ratio of 4 could improve aerodynamic performance when compared to a rigid counterpart. Flexible wings gave higher lift-to-drag ratios and drag was reduced significantly with slight changes in lift. Furthermore, it was found that the effective stiffness that improved aerodynamic performance was in a range of about 0.5–10, which corresponded to the wing stiffness of insects with similar aspect ratios. Chen et al.[33] investigated the aerodynamic model of 2D and 3D flexible flapping wings. Their results showed that the aerodynamic performance of a flapping wing during pitching flight and heaving flight could be improved significantly by the

asymmetric flexibility. This improvement was because the negative lift in the upstroke was alleviated by the twist deformation and positive camber of the wing. Agrawal and Agrawal[93] experimentally studied the aerodynamic performance of a flapping wing, which had the deformable behavior of a hawkmoth (Manduca sexta) wing. The flexible wing was constructed using a combination of materials (carbon, nylon, and rubber) for the veins and a latex membrane. They concluded that for all kinematic patterns, the thrust was increased by the flexible wing when compared to the rigid wing. In an experiment carried out by Wu et al.,[94] elasticity of flapping wing and thrust generation of six pairs of hummingbird-shaped membrane wings were presented. They summarized that for a certain spatial distribution of wing flexibility, it had an effective frequency range for thrust generation. At wing beat frequencies that thrust was produced, the important role of the wing flexibility was underlined, namely, bending and twisting deformation interacted with aerodynamic loads to enhance wing performance under a certain condition. Tobing et al.[26] also evaluated bumblebee propulsion under the effects of wing flexibility at an advance ratio of 0.2 and flapping amplitude of 16°. They indicated that uniform- and reduced tip stiffness wings produced averaged thrust with a difference of about 3%. Meanwhile, the rigid wing produced drag instead. Therefore, they stressed the importance of flexible wing for the aerodynamic performance and propulsion that a bumblebee could not fly forward if its wings were not modeled as deformable structures. This result was done similarly to an earlier work found by Nagai et al.,[95] who indicated that at this advance ratio, the bumblebee could only fly forward with trust producing, if it flapped with a higher amplitude of 60°. Lee et al.[29] investigated the flapping-wing characteristics under the effects of flexibility during hover and forward flight. They found that wing flexibility improved thrust with the increasing flapping frequency, as shown in Figure 22. However, the advance ratio was the cause of the thrust diminishment for flexible flapping wings, especially at high flapping frequency motions, as shown in Figure 23.

Deng et al.[96] numerically simulated the aerodynamic characteristics of single- and double-flexible flapping wings of DelFly. Their simulation showed that more aerodynamic force was generated by the double-wing flapping configuration during hovering flight. Namely, the double-wing case gave the averaged thrust coefficient of 0.3, whereas the single-wing cases provided a coefficient of 0.25. Besides, the thrust generated by both cases was equal approximately during the instroke phase. However, during the outstroke phase, the force was noticeably improved by double wings, as shown in Figure 24. This was explained by stronger LEV phenomena during the outstroke in the fling phase. However, the force enhancement was not observed by the

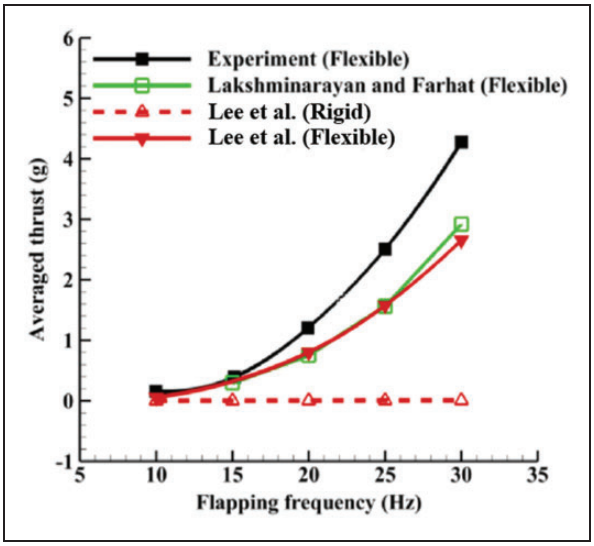

Figure 22. Aerodynamic performance in terms of averaged thrust response at different flapping frequencies.[29]

clapping mechanism because of the neutralized interaction from the wings at the end of the outstroke, as seen in Figure 25. The results also showed that during forward flight, the vortex structures at the velocity of 1, 2, and 3 m/s were qualitatively similar. However, they mainly changed in wavelength, namely, the wake was stretched and extended larger at a higher incoming velocity. In a most recent study, clapping and flinging motion of flapping wings was studied by Jadhav et al.[97] by means of force measurement and particle image velocimetry (PIV). They indicated that the clapping mechanism of the flexible wings barely contributed to lift enhancement since the momentum jet ejected from the trailing edge of the wings was low at the end of the clapping motion. Further force measurement and CFD simulations and in their work also revealed that the shorter distance between the wings at the end of clapping motion could provide higher lift enhancement due to the subsequent flinging motion. The flexible wings performed a larger lift enhancing LEVs during the fling motion after the shorter clapping distance. In addition, there have been several studies of the effects of wing flexibility on the aerodynamic performance and energy recovery by means of force measurement and analytic method. For instance, Pourtakdoust and Aliabadi[98] evaluated the propulsion system capabilities of a 3D membrane Flapping Micro Air Vehicle (FMAV) under a new aeroelastic model utilizing the Euler-Bernoulli torsion beam and quasi-steady aerodynamic model. Mazaheri and Ebrahimi[99] measured the aerodynamic performance of a 3D membrane flapping wing in terms of lift and thrust. Results from both studies indicated that the FMAV could reach optimum propulsive efficiency when the proper wing stiffness was used for the wings. Jankauski et al.[28] analytically investigated flapping-wing energetics

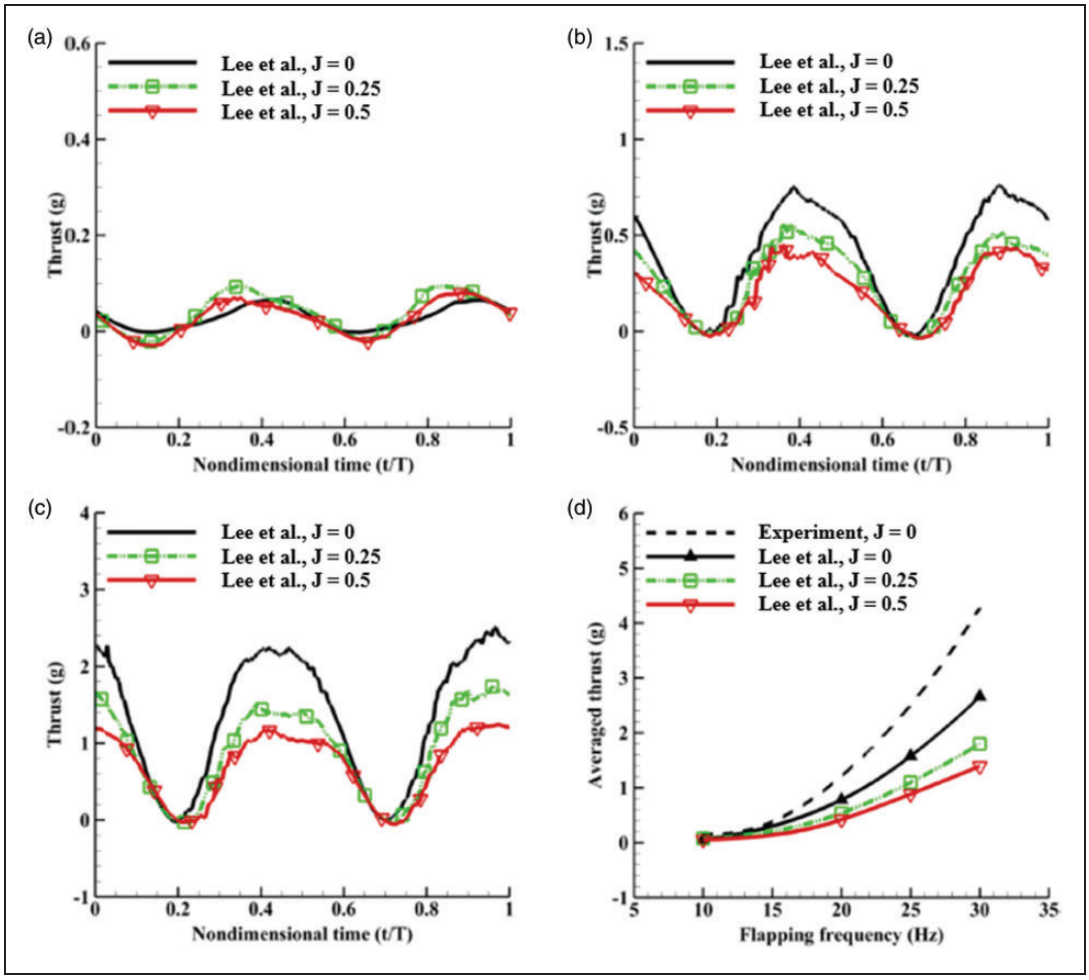

Figure 23. Aerodynamic performance with respect to the advance ratio: (a) thrust response with 10-Hz flapping motion, (b) thrust response with 20-Hz flapping motion, (c) thrust response with 30-Hz flapping motion, and (d) averaged thrust responses.[29]

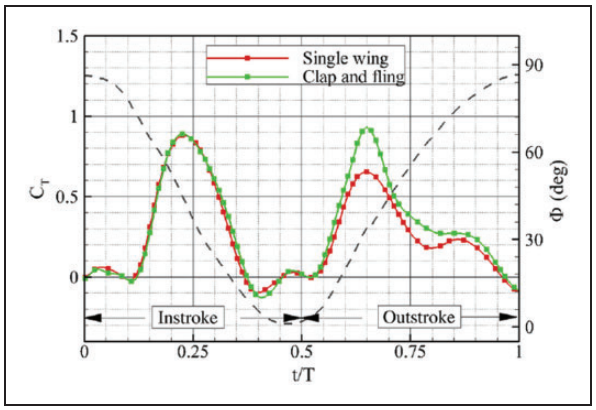

Figure 24. Thrust-coefficient enhancement by mechanism of clap-fling motion in hovering flight.[96]

under the effect of structural deformation. Results showed that considerable strain energy storage could be provided by wing deformation, and this energy could be reused for wing acceleration/deceleration during a flapping cycle. It was thought that this mechanism might reduce the inertial power requirements during flight. Also, they suggested that wing flexibility could decrease energetic expenditures. This corroborated the conclusions of several other researchers.[76,100,101]

Effects on wing acoustics

In nature, the sound of insects, such as bumbling sound or buzzing of bees, mosquitoes, or flies, is generated by its flapping-wing mechanism. This flapping sound generation in many kinds of insects including other biological flyers is considered as a byproduct of lift generation or a signal of mutual communication.[102–105] Besides, it is believed that this sound results from aerodynamic perform around the flapping wings such as LEV, TEV, and TV caused by the complex fluid–solid interaction between the flapping wings and the flow field,[106,107] including other parameters such as wing geometry and flapping amplitude.[105] This sound is considered as aeroacoustics and a scaling analysis[105] is presently supplemented to understand the quantitative relations of the mean lift, mechanical power, and sound power. This analysis shows that flapping wing could operate at (1) a lower flapping frequency, (2) larger stroke amplitude,

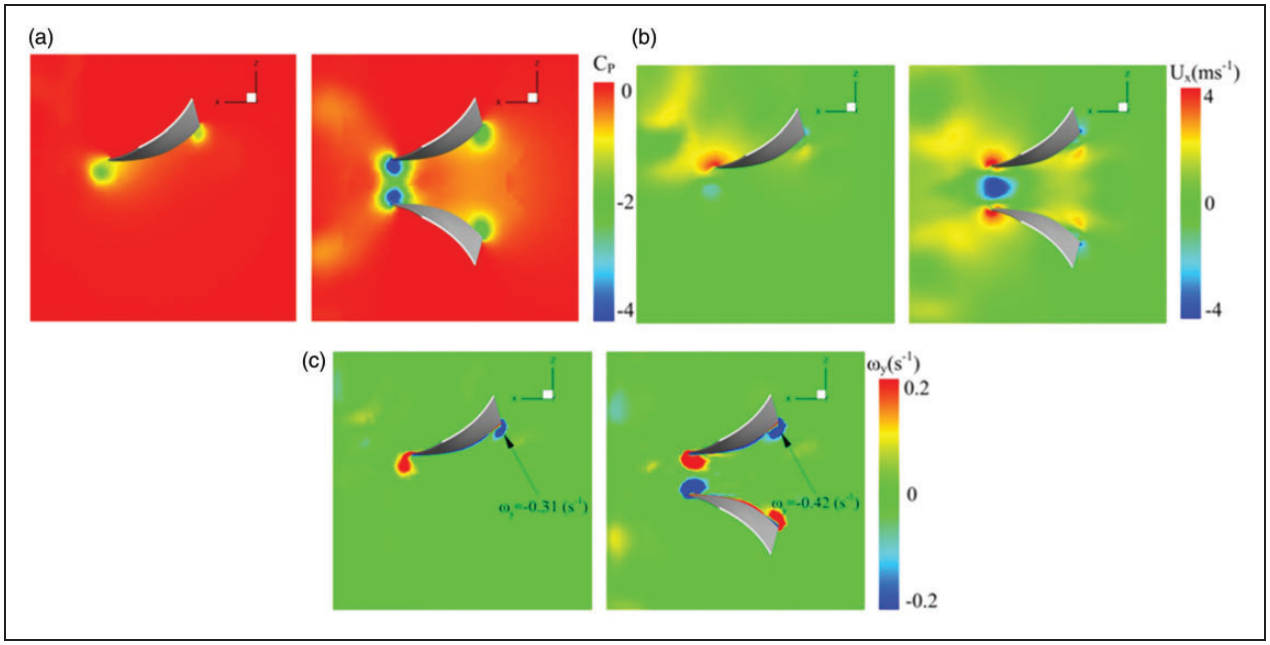

Figure 25. Flow fields between single and clap-fling configurations at t/T = 0.7: (a) pressure, (b) velocity in x-direction, and (c) vorticity in y-direction; slice shown was located at 70% chord.[96]

and (3) lower wing aspect ratio to reduce the noise produced by the wing while continuing the same aerodynamic performance. In fact, the natural phenomena are complicated because wings of biological flyers or insects involve wing flexibility.[32,46,47,108] The structure of a flexible wing undergoing the flapping mode, which is like vibration of the structure, may cause some of the energy from the structure to escape into the air, some of which emits as a vibroacoustic sound. The fluctuation of spatial and temporal air pressure which is caused by these phenomena propagates spherically as a sound wave. In this section, it further reviews from the earlier section, reviewing the flexibility effects on aeroacoustics is presented through open literature to obtain a comprehensive understanding of phenomena of the sound generation and its propagation, mechanism, and function. This can suggest how to control and function the noise generated by insect-like MUAVs and UAVs for the perfect design of biomimetic applications, namely, MAVs and MUAVs should have the high-aerodynamic performance like insect flight but low noise.

Following the rapid and dynamic growth of CFD approaches, the prediction of computational aeroacoustics (CAA) is basically succeeded using three groups of the numerical technique. First, the hybrid approach is introduced and according to the name, the computational domain is split into different regions so that the governing equations are solved for the flow and acoustic fields, respectively. The flow field in terms of the velocity and pressure of flapping wings obtained from solving the Navier–Stokes equations can be done by steady-state or transient analysis. The flow field is then used to calculate sources of aeroacoustics. The governing equation of acoustics is solved through the acoustical sources for the sound propagation using several methods such as Lighthill's analogy,[109] and the Ffowcs–Williams–Hawkings (FWH) equation.[110] Second, the direct numerical simulation (DNS) is a CAA approach based on the compressible Navier–Stokes equation. With this approach, the flow field and the aerodynamically generated acoustic field in near and intermediate ranges are solved directly. The advantage of the DNS is that the sound calculation is not limited by the low range of Mach number and compactness of source region (near-field acoustics).[111] Nonetheless, high computational resources are required. Third, the CAA is calculated using an acoustic/viscous splitting technique.[112] In this technique, the calculation of the compressible viscous flow is decomposed into the time-dependent calculation of an incompressible flow and the calculation of a perturbed compressible flow. Then, the acoustic results are considered by the fluctuation in the far field.

In this review, the FWH equation that is based on Lighthill's acoustic analogy and DNS are summarized below as presently they have been widely employed by several groups of researchers for CAA in biomimetic flyers, MUAVs, and MAVs, which will be mentioned in the subsections of this part.

1. FWH:

The velocity and pressure of flapping wings obtained from the Navier–Stokes equations are used to evaluate the sound pressure by solving the FWH equation, as seen in equations (34) to (38).[105,110,113]

Then, the sound pressure level (SPL) can be calculated from the acoustic pressure in equation (39).

$$P_{ac}(r,t) = P_{\text{thickness}}(r,t) + P_{\text{loading}}(r,t) + P_{\text{turbulence}}(r,t) \tag{34}$$

$$P_{\text{thickness}}(r,t) = \frac{1}{4\pi}\frac{\partial}{\partial t}\int \frac{\rho v_n}{r\Lambda}\mathrm{d}\sum \tag{35}$$

$$P_{\text{loading}}(r,t) = \frac{1}{4\pi c_o}\frac{\partial}{\partial t}\int \frac{p_b\cos\sigma}{r\Lambda}\mathrm{d}\sum + \frac{1}{4\pi}\frac{\partial}{\partial t}\int \frac{p_b\cos\sigma}{r^2\Lambda}\mathrm{d}\sum \tag{36}$$

$$P_{\text{turbulence}}(r,t) = \frac{\partial^2 T}{\partial x^2} \tag{37}$$

$$\Lambda = \sqrt{1 + Ma^2 - 2Ma\cos\sigma} \tag{38}$$

$$SPL = 20\log\left(\frac{P_{ac}}{P_{Ref}}\right) \tag{39}$$

where Ma is the Mach number. In flapping flight, Mach number may be very small and hence $\Lambda = 1$. p_b denotes the pressure distribution, r is the distance from sound source, which usually is the geometric center of the wing, to the observer, v_n stands for the velocity normal to the wing surface, σ represents the angle between the vector normal to the wing surface and the vector at observer position, c_o is the sound speed, S is the wing surface, and P_{Ref} is the reference pressure. In FWH equation, the acoustic pressure is calculated from pressure under the influence of wing thickness, wing air loading, and turbulence of flow around the wing. This leads to the incorporation of monopole, dipole, and quadrupole sound sources. However, the quadrupole source is often ignored because the acoustic power of the quadrupole source is insignificant at low Mach-number conditions which match the flapping motion of insects.[104] More details about the application of the FWH equation to other problems can be seen in Guo.[114]

2. Direct numerical simulation (DNS):

The DNS directly solves transient compressible Navier–Stokes equations using high-order schemes of the combination of aerodynamic and acoustic fields for the acceptable accuracy of the pressure fluctuation. Then, the SPL and its spectrum can be predicted. With DNS, some difficulties obtained from the hybrid approaches can be averted such as the match between different numerical methods.[115] The full transient-compressible Navier–Stokes equations, as expressed in equations (40) to (42), are solved by the DNS[116] and all scales are resolved down to the Kolmogorov length.

$$\frac{\partial\rho}{\partial t} + \frac{\partial(\rho u_k)}{\partial x_k} = 0 \tag{40}$$

$$\frac{\partial(\rho u_i)}{\partial t} + \frac{\partial(\rho u_i u_k + p\delta_{ik} - \tau_{ik})}{\partial x_k} = 0 \tag{41}$$

$$\frac{\partial(\rho E)}{\partial t} + \frac{\partial\left(\rho u_k\left[E + \frac{p}{\rho}\right] + q_k - u_i\tau_{ik}\right)}{\partial x_k} = 0 \tag{42}$$

where

$$E = \frac{T}{[\gamma(\gamma-1)Ma^2]} + \frac{1}{2}u_i u_i \tag{43}$$

$$\tau_{ik} = \frac{\mu}{Re}\left(\frac{\partial u_i}{\partial x_k} + \frac{\partial u_k}{\partial x_i} - \frac{2}{3}\frac{\partial u_j}{\partial x_j}\delta_{ik}\right) \tag{44}$$

$$q_k = -\frac{\mu}{(\gamma-1)Ma^2 PrRe}\frac{\partial T}{\partial x_k} \tag{45}$$

$$p = \frac{\rho T}{\gamma Ma^2} \tag{46}$$

Here, Pr is the Prandtl number and μ is the molecular viscosity which is computed using the law of Sutherland.

For biomimetic flyers, the acoustic pressure generated by rigid or flexible flapping wings is commonly calculated by the immersed boundary method (IBM) due to its advantage in the moving-body calculation.[105,108,117] To further simulate and approach natural of sound generation and propagation of biological flyers, Wang and Tian[108] and Wang et al.[117] introduced the simultaneous computation of DNS and IBM for aerodynamic and acoustic solutions of fully fluid-structure–acoustics interaction in problems with large deformations and complex geometries. The governing equations of fluid dynamics and the flexibility of deformable structures are solved independently. The interaction force between the fluid and structure, as expressed in equation (47), is computed explicitly using a feedback law[118] based on the penalty immersed boundary (pIB) method.

$$\mathbf{F}_f = \alpha\int_0^t(\mathbf{U}_{ib} - \mathbf{U})dt + \beta(\mathbf{U}_{ib} - \mathbf{U}) \tag{47}$$

where

$$\mathbf{U}_{ib}(s,t) = \int_V \mathbf{u}(x,t)\delta_h(\mathbf{X}(s,t) - \mathbf{x})\mathrm{d}\mathbf{x} \tag{48}$$

$$\mathbf{f}(\mathbf{x},t) = -\int_\Gamma \mathbf{F}_f(s,t)\delta_h(\mathbf{X}(s,t) - \mathbf{x})\mathrm{d}s \tag{49}$$

$$\delta_h(x,y) = \frac{1}{h^2}\lambda\left(\frac{x}{h}\right)\lambda\left(\frac{y}{h}\right) \tag{50}$$

Here, $\mathbf{U}_{ib}$ is the integrated boundary velocity in the flow, $\mathbf{U}$ is the velocity of the structure, and α and β are constants with a large positive value. $\mathbf{u}$ is the fluid velocity, $\mathbf{X}$ is the structural-node coordinates, $\mathbf{x}$ is the fluid coordinates, s is the arc coordinate for a 2D domain, V is the fluid domain, Γ is the structure domain, and δh is the smoothed Dirac delta function as reported by Peskin.[119] In addition, aerodynamic sound can be calculated by means of analytic approaches as well.[45,47] As summary, the recent studies on the effects of flexibility on wing acoustics are listed in Table 4 with key factors, acoustic investigations and methods.

Two-dimensional analysis

Weidenfeld and Manela[45] investigated the acoustic field of a thin flexible filament which was hanging and undergoing small-amplitude harmonic heaving motion under uniform mean flow parallel to itself, high Reynold number, and low Mach number. Based on the Powell–Howe acoustic analogy, a discrete-wake model with the thin airfoil theory was used to set the source term for a near-field sound prediction, and then a Greens function approach was used for the far-field sound calculation. Their results indicated that a highly elastic filament generated the acoustic field which converged to the far field of a hanging membrane in the limit of small flexural stiffnesses. In general, the membrane generated the highest sound levels and bending stiffness in highly elastic configurations was prone to suppress the sound level generated by the system. The role of the wake sound contribution was introduced for these phenomena, also. Purohit et al.[46] numerically studied aerodynamic sound in the far field under the effects of flexibility at $\mathrm{Re} = 200$ and $\mathrm{Ma} = 0.1$ using an aeroacoustic hybrid method with two-step computational technique and a surface source method based on the Euler equations. A trailing splitter plate at the tail of a bluff body was used for sound generation. The plate was excited by upstream vortices generated by the bluff body. Their results revealed that the flexibility caused the vortex field significantly and led to an effect on the far-field aerodynamic sound. Additionally, the flexibility increased sound pressure and shifted the directivity pattern when compared to the rigid plate, as seen in Figures 26 and 27. A further study done by Purohit et al.[120] highlighted the role of flexibility effects in the aerodynamic sound produced from a flow-induced vibration of the elastic plate under external harmonic forced excitation. They indicated that the harmonic force excitation of the flexible plate, such as amplitude and frequency, has a great impact on resultant far-field aerodynamic sound. In addition, it was found that the presence of external excitation affected the flow pressure and acoustic pressure characteristics of the unforced vibrating structures in the flow field.

Another role of the flexibility in acoustics was done by Manela[121] and Manela and Halachmi[122] they showed that wing flexibility was an important factor when the acoustic sound was considered as it could play a major role as sound generation damping or amplification based on the actuating frequency of the wing.[121,123] In recent work, Springer et al.[124] investigated fluid-structure–acoustic coupling for a flexible flat plate installed behind a step. Results indicated that vibroacoustic sound propagation was based on the temporal displacement of a flexible plate located in the wake region of the step, loaded with turbulent pressure and shear stress forces. Results also showed a strong influence of the interaction between structural deformation and acoustic medium, including considerable damping effects on the structural deformation. Wang and Tian[108] examined the combined interaction of fluid structure and acoustics of flexible flapping wings at a Reynolds number of 100 and Mach number of 0.1 using a technique of the DNS and fast Fourier transform (FFT) at a distance of 40L; L = chord length. Results showed that the lift had an important role in sound production and the sound directivity was observed in an eight shape, and the direction of the sound shifted clockwise, as seen in Figure 28. This figure also indicated that the flexibility (ω*) (1) increased the RMS values of the fluctuating pressure in all directions, (2) transformed the acoustic field from dipole directivity to monopole directivity, and (3) enhanced the shift of sound directivity. The results also presented the flapping frequency (f_0) and its double ($2f_0$) obtained by the FFT analysis of the fluctuating pressure. This analysis indicated that f_0 was found in the vertical direction, whereas $2f_0$ and performed in the horizontal direction. In addition, the fluctuating pressure at f_0 and $2f_0$ was plotted in the polar diagram and it indicated that the fluctuating pressure at f_0 was a dipole one, as shown in Figure 29(a). The diagram also showed the shift effects at $2f_0$ and the slight decrease in the maximum sound along the circumference caused by the wing flexibility, as seen in Figure 29(b). They deemed that this corresponded to the clockwise shift since the increment in the amplitude of the thrust and bending deformation, which was caused by the flexibility, was significant, as shown in Figure 30(b). Besides, it was observed that the resultant effects caused by the thrust and lift dominated the maximum fluctuating pressure.

Nedunchezian et al.[125] used the FWH equation to evaluate the sound pressure of a 2D wing with the fruit-fly scale in hovering flight at $\mathrm{Re} = 100$ and $\mathrm{Ma} \approx 0$. They indicated that the SPL_{max} strongly depended upon the effective stiffness and the reduced frequency number of the wing, as seen in Figure 31(a) and 31(b), respectively. This suggested that wing flexibility was a key factor in reducing the sound generation. A relationship among kinematics, aerodynamic force, and the sound was drawn in their results, also.

Table 4. Aeroacoustics of flapping-wing flyers summarized category of flexibility study.

Ref.	Model	Motion mode	Re/Ma	Acoustic investigation	Method
(a) 2D model					
[45]	2D thin filament	Hanging/harmonic heaving motion	High Re and low Ma	Sound generation, acoustic far field	Thin airfoil theory and a discrete wake model/ Powell–Howe acoustic analogy/compact greens function
[46]	2D plate	Vertical vibration/ forced externally	$Re = 150\, M = 0.1$	Sound generation, Aerodynamic far field sound, directivity	Two-step computational aeroacoustic hybrid method/linearized Euler equation based on surface injection method
[47]	2D plate	Vibration caused by a vortex convected	High Re and low Ma	Sound generation, acoustic far field sound	Chebyshev collocation method/compact greens function
[108]	2D plate	Translation/rotation	$Re = 100\, Ma = 0.1$	Sound generation, directivity in far field	Direct numerical simulation/Fast Fourier transform (FFT)
[120]	2D plate	Vertical vibration/ unforced externally	$Re = 200\, M = 0.1$	Sound generation, aerodynamic far field sound, directivity	Two-step computational aeroacoustic hybrid method/Linearized Euler equation based on surface injection method
[121]	2D plate	Vibration caused by actuated at leading edge	high Re and low Ma	Sound generation, acoustic far field sound	Chebyshev collocation method/wave equation/ compact greens function
[122]	2D plate	Harmonic pitching	high Re and low Ma	Sound generation, acoustic far field sound	Thin airfoil theory/Powell Howe acoustic analogy/ compact greens function
[124]	2D plate	Vertical vibration	$Re = 26{,}000$	Sound generation, vibroacoustic near field	Large eddy simulation/Lighthills acoustic analogy/ wave equation
[125]	2D fruit fly-like	Hovering flight	$Re = 100\, M \approx 0$	Sound generation, directivity	Ffowcs–Williams–Hawkings (FWH) Model
(b) 3D model					
[32]	3D Tibicen linnei cicada-like	Forward flight	$Re = 3500\, Ma < 0.04$	Sound generation, directivity and sound pressure level (SPL) in far field	Direct numerical simulation/fast Fourier transform (FFT)/linearized perturbed compressible equation (LPCE) based on hydrodynamic/ acoustic splitting method
[127]	3D Tibicen linnei cicada-like	Forward flight	$Re = 3500\, Ma < 0.04$	Sound and force production	Direct numerical simulation/fast Fourier transform (FFT)/linearized perturbed compressible equation (LPCE) based on hydrodynamic/ acoustic splitting method

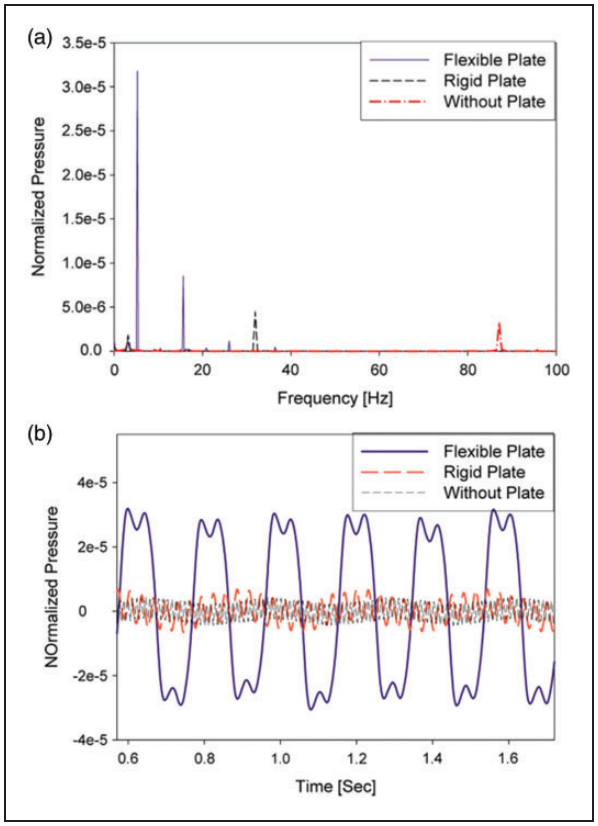

Figure 26. Comparisons of three cases for (a) normalized pressure (p'/p_∞) against time and (b) normalized pressure at distance 400 L against frequency spectrum; L = side length of bluff body.[46]

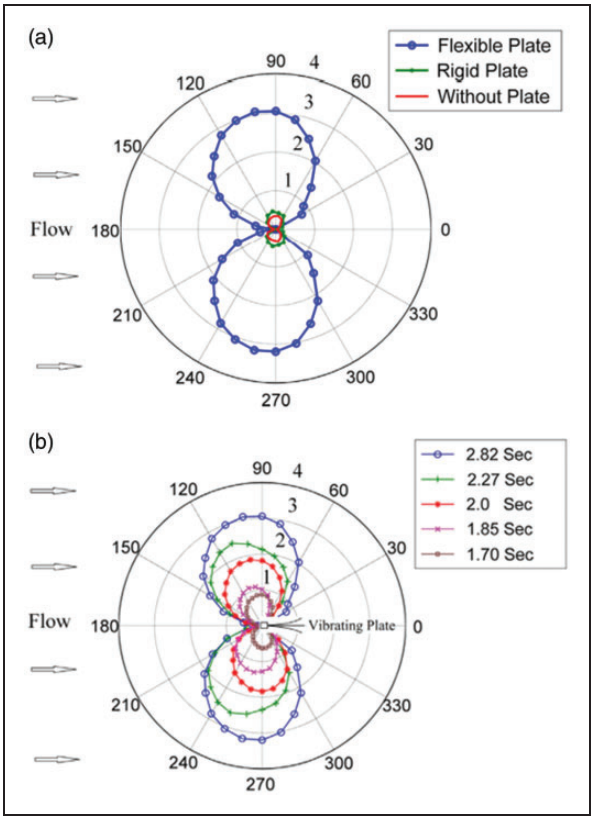

Figure 27. (a) Sound pressure directivity for the three cases and (b) sound pressure distribution for flexible plate at radial distance of 400 L at different times; L = side length of bluff body.[46]

With the reduced frequency number of 0.3 and effective stiffness of 0.42, it provided the highest efficiency of 0.56, a low power requirement of 1.8, and a relatively high lift of 1.0, thereby causing the SPL_{max} of 80.5 dB, which agrees well with the measurements of fruit flies reported by the reference.[126] They suggested that the biological flyers might fly with high efficiency and low acoustic production instead of the motion with the highest force generation so that it could consume low power and lower sound production. In addition, the highest SPL_{max} of 85dB was found at the highest lift of 3.3.

Three-dimensional analysis

So far, very little contribution to sound generation and its propagation and mechanisms produced by flapping wing flyers have given when wing flexibility is taken into account, particularly in the 3D model. As far as we know, only computational work was conducted by Geng et al.[32] They studied the unsteady flow and characteristics of far-field acoustic of a 3D flexible-wing model; Tibicen linnei cicada like at a distance of 75c in spherical direction, where c = chord, during forward flight. They found that flapping sound was directional, the dominant frequency varied around the wing. The pattern of acoustic distribution matched the pattern of aerodynamic distribution very

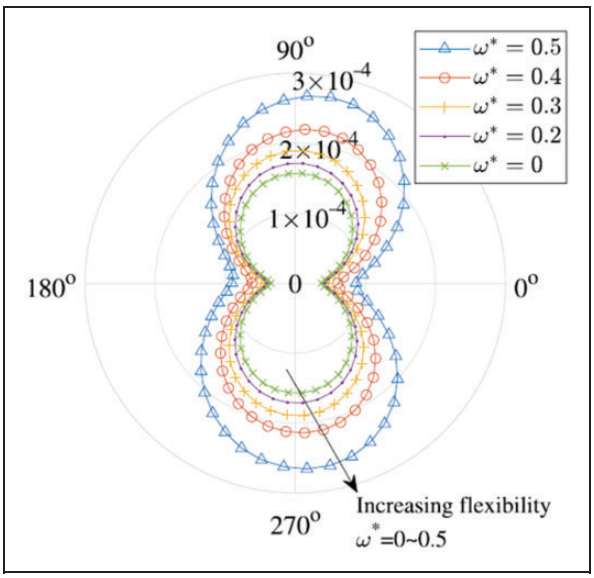

Figure 28. Sound directivity generated by flexible wings at distance of 40L; ω^* denotes frequency ratio obtained by combining bending rigidity in calculation, so it represents flexibility effect.[108]

well for f for the flexible wing and both f and $2f$ for the rigid wing. However, the dipole axis change of the pressure perturbation for the flexible wing might lead to a mismatch of $2f$ pattern, as shown in Figures 32 and 33. Another observation from the

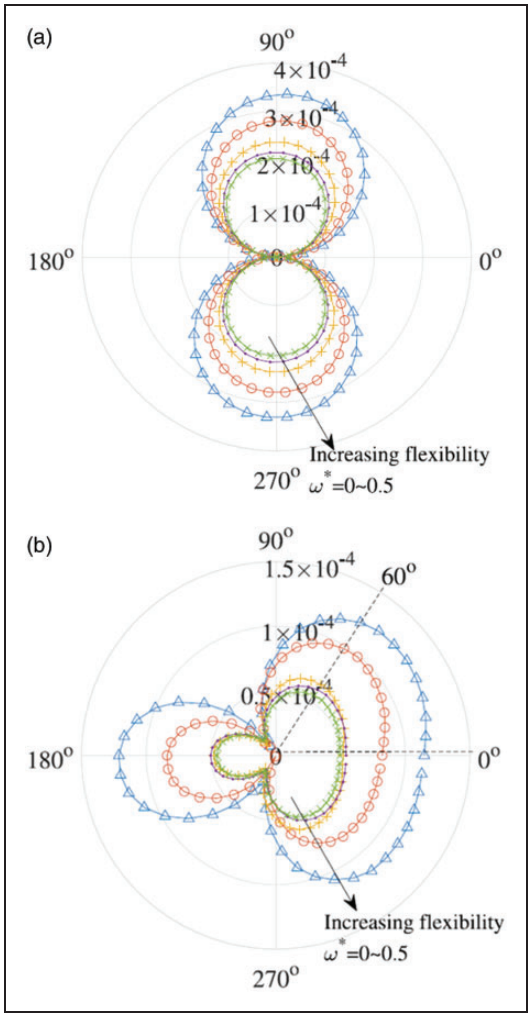

Figure 29. Polar diagram of fluctuating pressure at distance of 40L at (a) f_0 and (b) $2f_0$ when Re = 100, $\omega^* = 5.0$, $\beta = 45^\circ$, $\alpha_m = 45^\circ$, Ma = 0.1, and $U_r = 1.0$.[108]

figures was that the first and second modes of harmonic frequency showed a different pattern of sound propagation between the rigid and flexible wings because of highly complex phenomena from wing kinematics and loadings. Furthermore, the rotation and deformation in the flexible wing were found to help lower the sound strength in all directions. They also indicated that directivity obtained from both f and 2f showed a dipole-like pattern in 3D, but the direction of the dipole axis was different. The flexible wing results in the dipole axis shift and SPL reduction for both frequencies when compared to the rigid counterpart. With the same wing model, Geng et al.[127] further studied the effects of wing flexibility by investigating the generation of flapping noise and force simultaneously. They found that the flexible wing generated lower sound in all directions because the wings produced lower aerodynamic forces and the directivity of the flapping tone changed gradually with the wing flexibility, as seen in Figures 34 and 35. Besides, they pointed out the relationship between aerodynamic forces and dynamic pressure forces. Specifically, the aerodynamic forces scaled with the dynamic pressure force. In Figure 35(a) and 35(b), one could observe that the relative magnitudes of the aerodynamic forces and dynamic pressure force for each model were similar in general for both downstroke and upstroke. However, the flexible models produced higher aerodynamic forces but lower dynamic pressure forces than the rigid model in the y-direction for the downstroke. These phenomena suggested that the kinematics of the flexible-wing models played both positive and negative effects on the forces, namely, even though it reduced the dynamic pressure force, it maintained the high lift during downstroke. The reason might be explained by the fact that the primary mechanism of lift generation during downstroke was LEVs, which were affected by the vortex dynamic rather than the dynamic pressures.

Recommendation

Aerodynamic aspect

Although studies of the flexibility effects on wing aerodynamic performance have been conducted for a very long time for biomimetic flyers, MUAVs, and MAVs, there are still a lot of aspects available for design improvement. Some recommendations for the aerodynamic aspect under the wing-flexibility effects are given for the future development of the biomimetic flyers, MUAVs, and MAVs.

1. According to the review, most of the researches conducted investigations of biomimetic flyers, MUAVs, and MAVs either experimental or numerical approaches, only the part of wings was considered. This isolated wing study is insufficient because the flapping-wing motion has an impact on other parts of the flyer body and vice versa. Therefore, using multi-body dynamics is needed for a more accurate analysis, thereby improving the prediction of aerodynamic performance.
2. Because the body part of most biological flyers and insects, which is likely to be the biggest part, is not rigid indeed, so the body flexibility may have to be considered and only the body angle in body kinematics seems insufficient for its description.
3. In natural, biological flyers must survive under changeable environments such as rainy, snowy, windy, and sandy. It seems that only wind gust is taken into account. Studies of other environmental factors like flight under the rain, snow, or even cross-wind gust are limited. An effort to contribute toward this kind of study is still challenging for durable biomimetic flyers, MUAVs, and MAVs design.
4. As well known about the favorable and unfavorable effects of LEVs, TEVs, and TVs from a

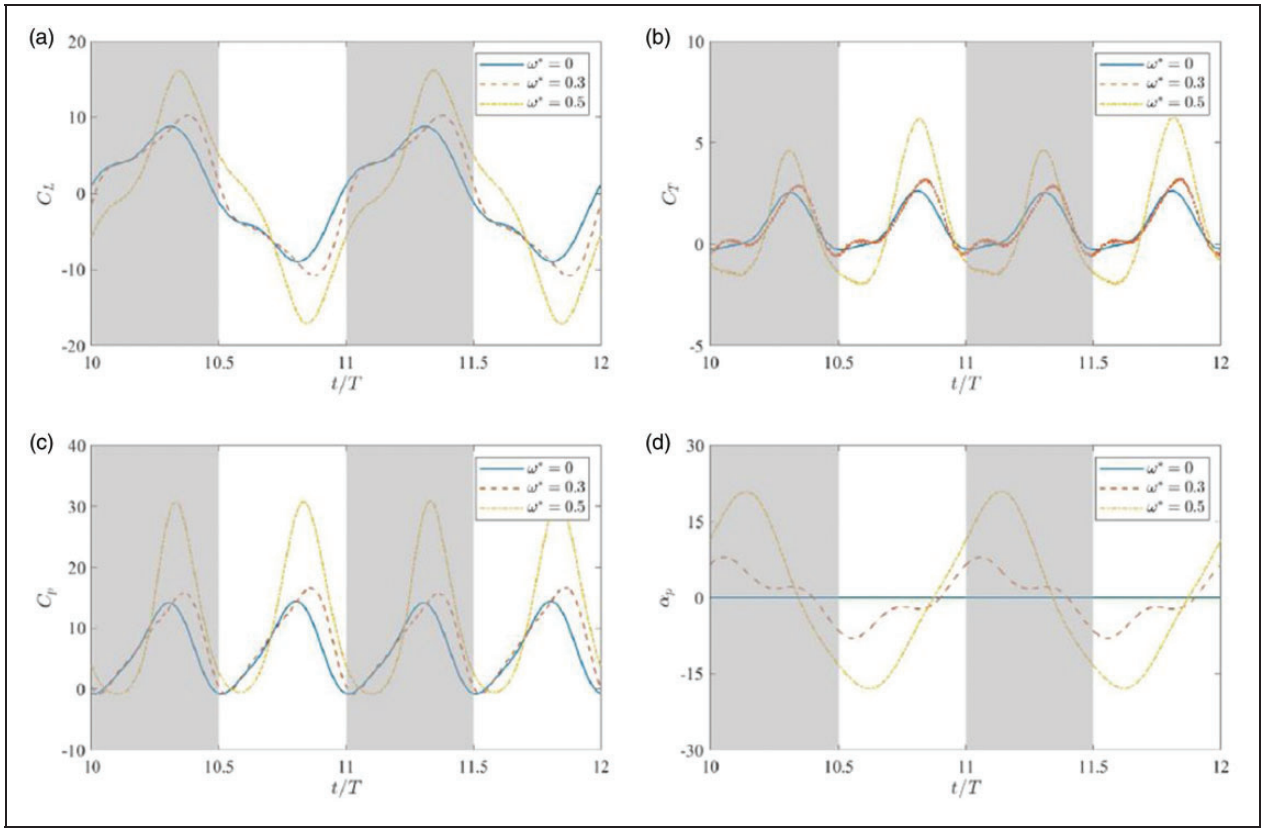

Figure 30. Time histories of (a) C_L, (b) $C_{\bar{n}}$ (c) C_p, and (d) α_p when Re = 100, $\alpha_m = 45^\circ$, $\beta = 90^\circ$, Ma = 0.1, and $U_r = 1.0$. White and gray and regions indicated upstroke and downstroke, respectively.[108]

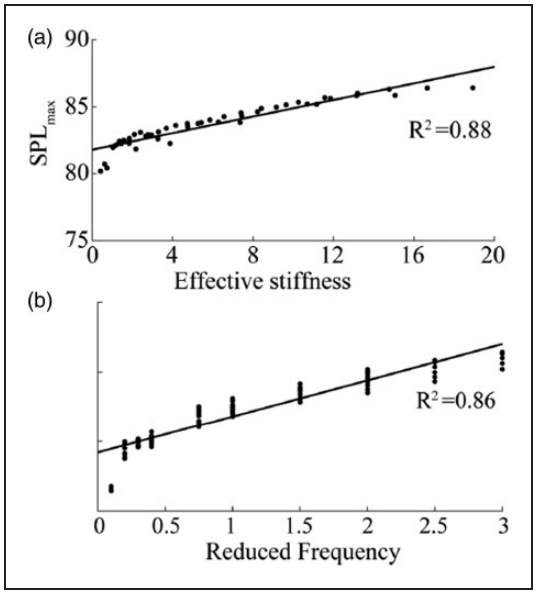

Figure 31. Correlation between SPL_{max} and (a) effective stiffness and (b) reduced frequency number.[125]

flexible wing on the aerodynamic performance in terms of lift, thrust, efficiency, and power consumption, searching for methods to increase this favorable effect and reduce the unfavorable effect is still important. Besides, more active control utilization for a desired aerodynamic performance needs to be used.

5. Energy extraction under wing flexibility is insufficiently understood. Further studies of this mechanism and its function can lead to better utilization of power storage and recovery of biomimetic flyers, including MUAVs and MAVs.
6. Although many pieces of open literature have studied the wing flexibility under hovering and forward flights, research on transition flight, which involves flow physics around wings and body, such as flight mode between hover and forward flight, from rest to takeoff/landing vertical in an arbitrary plane in 3D space is limited. Thus, the research on these conditions can provide future innovations in biomimetic flyers, UMAVs, and MAVs with multipurpose applications.
7. A few comprehensive data based on experiments in aerodynamic performance under the wing flexibility have been provided. Thus, the experimental study needs to grow. For example, the references[16,78,79,128] used PIV techniques to analyze the flow field around the flapping wing.
8. Implementations of the fluid–solid interaction are limited. Development of the numerical approach, such as the IBM, to further study and obtain accurate results of the full fluid–solid interaction of biomimetic flyers is still needed. This can be seen in a comprehensive review done by Deng et al.[129] and Huang and Tian.[130]

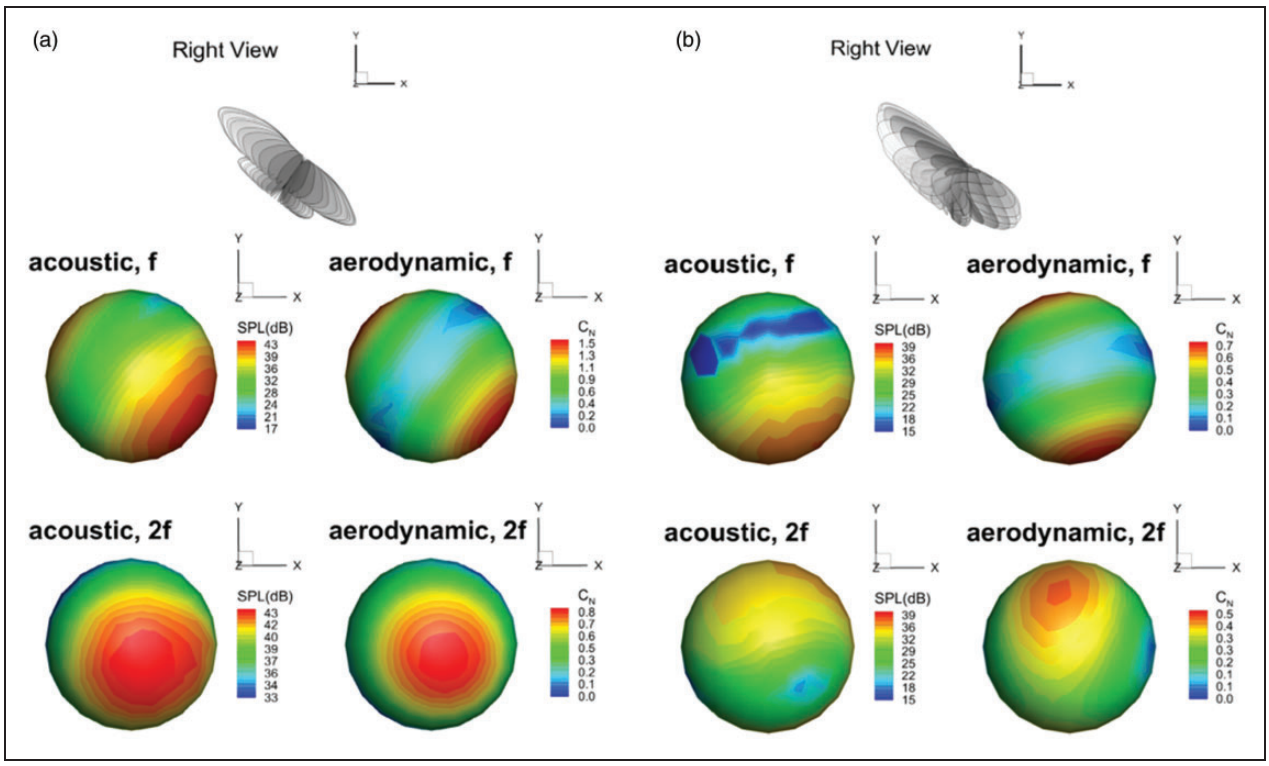

Figure 32. Comparisons of acoustic and aerodynamic patterns using *SPL* and C_N, respectively for (a) rigid flapping plate and (b) flexible flapping plate.[32]

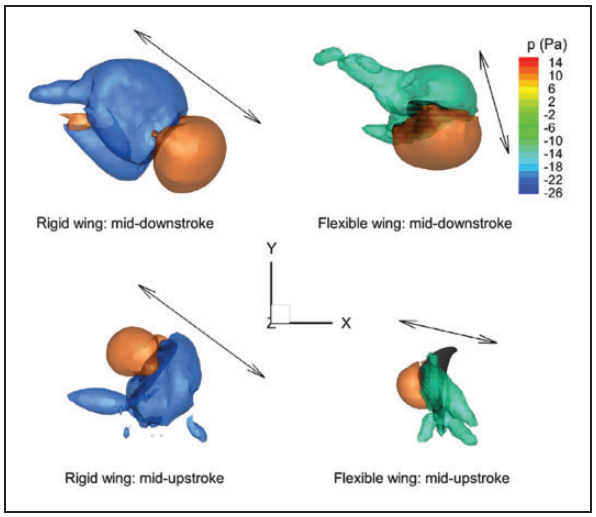

Figure 33. Iso-surface pressure at two sides of wing. Arrows indicated pressure perturbation direction at time instant.[32]

9. Optimal and robust designs for geometry and its kinematics, material properties, flight conditions, including environmental factors are required. These designs request close coordination of combined computational and experimental investigations.

Acoustic aspect

To reach a highly effective performance of the flyers, noise generated by flexible wings needs to be coupled to aerodynamic performance simultaneously. Unfortunately, due to very little contribution to a problem of flexible wings, the effects of the flexibility on acoustics have not been well understood so far. Consequently, this problem still opens widely and challenges both experimental and computational approaches for studying this inherently integrated interaction. The following recommendations are given for the acoustic aspect under the wing-flexibility effects.

1. A 3D study of the fluid structure acoustics interaction should be extended experimentally and computationally because flexible wings are under the significant influence of the combined deformations in the chordwise and spanwise directions. This will provide more useful data of the flapping-wing motion with the fluid structure acoustics interaction to obtain a comprehensive understanding of biological flights, thereby improving the design of insect-like flyers, MUAVs, and MAVs for the real flight of biological flyers.
2. To be detailed, the interplay between the kinematics, resultant aerodynamic forces and structural dynamics, and sound generation of a flexible wing undergoing flapping flights needs to be investigated more to elucidate the relation between the kinematics, aerodynamics, and acoustics of the wing under the flexibility effects.
3. Besides, sound generation and propagation mechanism based on macroscopic and microscopic

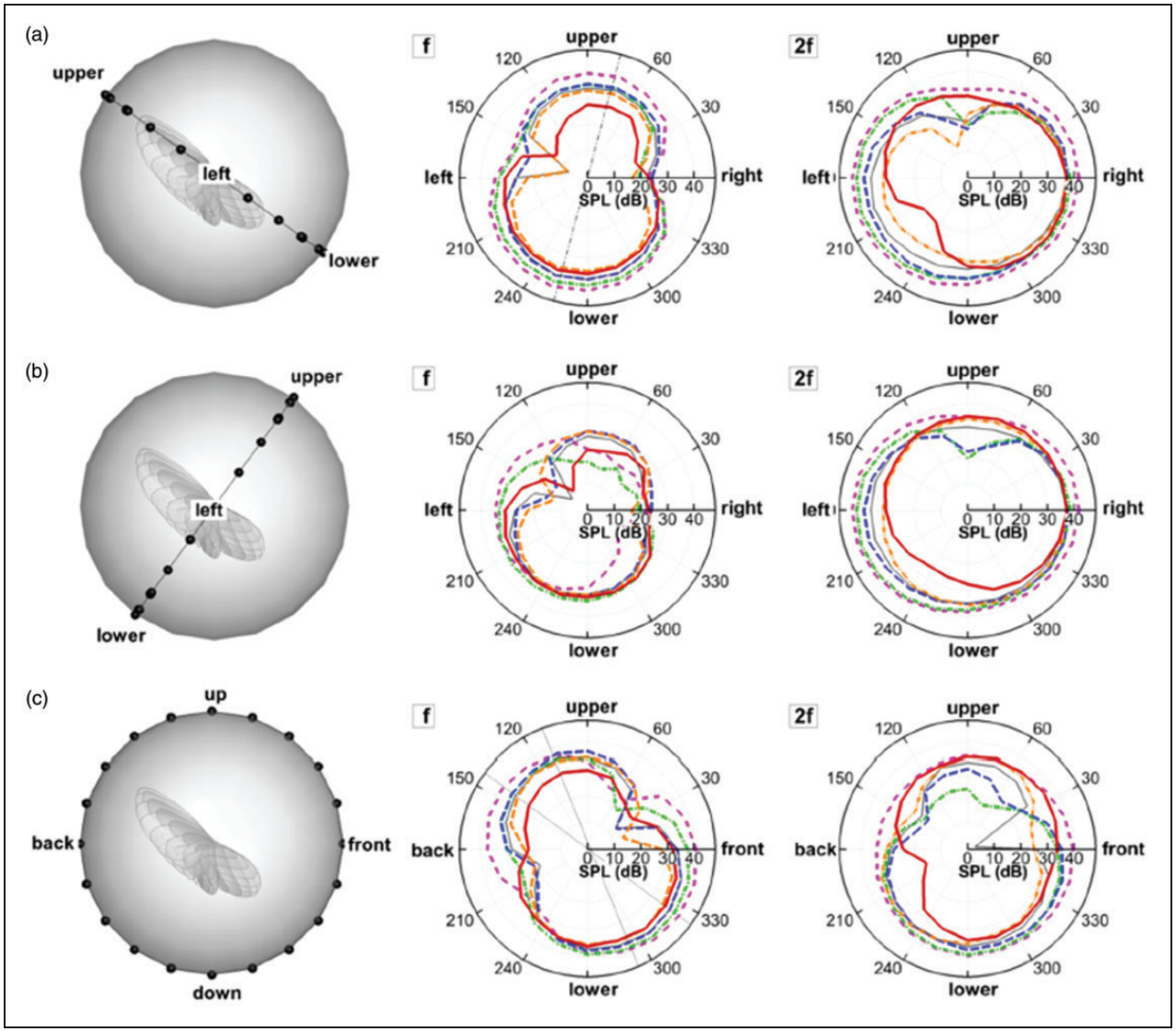

Figure 34. *SPL* distributions of all models for each of harmonics at r = 75c in (a) stroke plane, (b) perpendicular plane, and (c) saggital plane; violet for M1, green for M1 + 0.50M2, blue for M1 + 0.75M2, gray for M1 + 1.00M2, orange for M1 + 1.25M2, and red for real motion.[127]

views under the wing flexibility are still insufficient. Research in these issues can increase understanding of sound-wave phenomena produced by a flexible wing, thereby leading to other acoustic applications of flyers and ways to control and function this sound.

4. Based on the numerical approach, the improvement of stable and accurate numerical techniques for CFD/CAA is still needed, especially in flexible-wing problems using DNS. Usually, DNS requires high-order schemes with low dissipative and low dispersive errors in space and time, including well-designed boundary conditions for accurate prediction of sound generation and propagation to the far field. However, instability is commonly observed. Therefore, ways of alternative schemes with some interest are still open such as optimized low-dispersion schemes and their development that are developed for instability reduction with acceptable accuracy of computational results.[131–133]
5. As the recommendations are given in (1)–(4), although very little open literature has been reviewed, it was done by means of numerical approaches. There is a serious shortage of experimental studies for this problem. Therefore, the experimental study needs to be carried out more because benchmark experiments are used to develop accuracy of numerical results predicted by CFD codes.
6. As it is known that the structure of a biological wing is anisotropic and cambered under the flexibility, the flexural distribution of the wing is likely to cause not only aerodynamic performance but also wig acoustics. These considerations should be addressed as well.
7. The analysis of flexible wing acoustics is still critical to the future of biomimetic flyers due to the

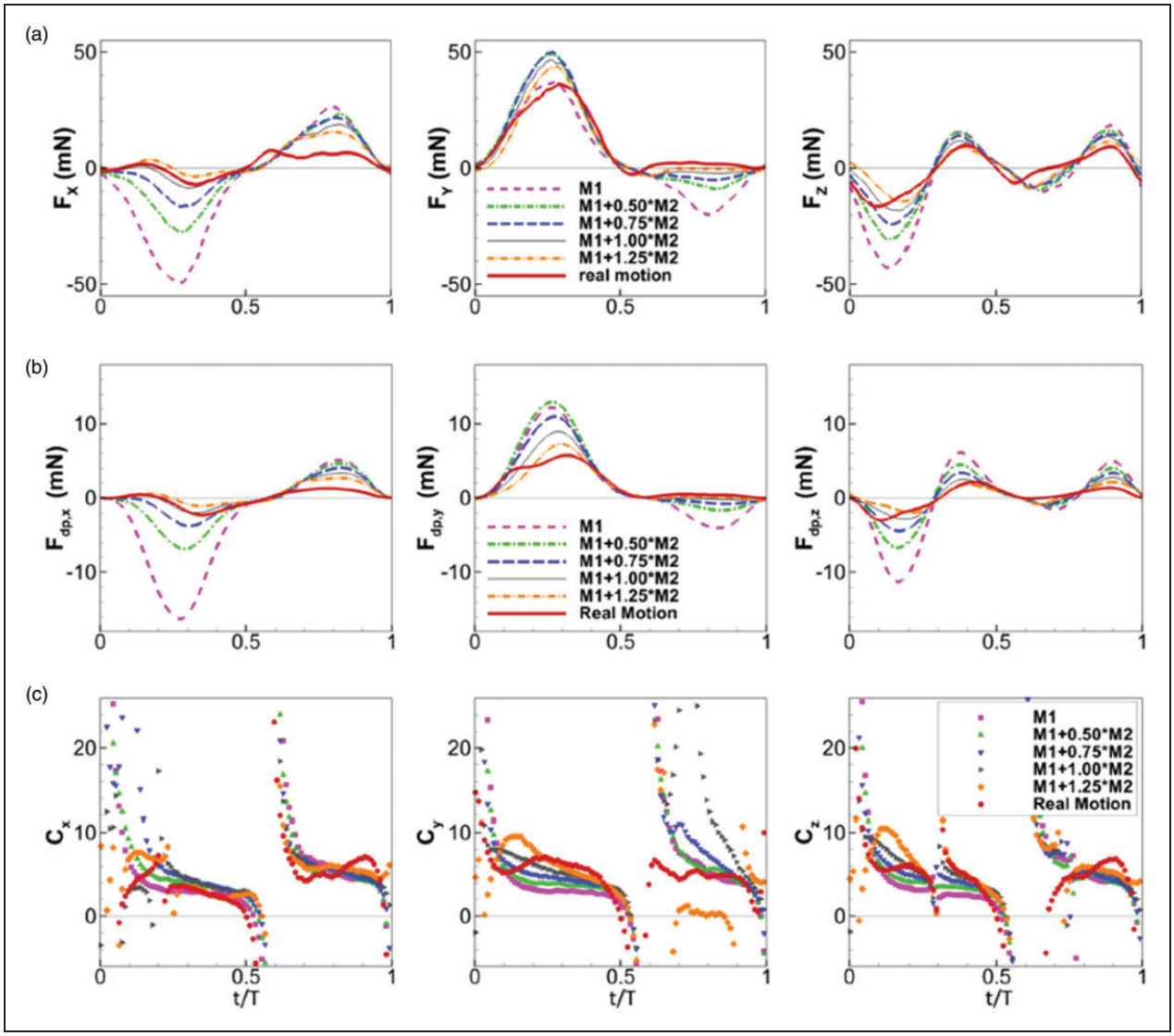

Figure 35. Comparisons of (a) aerodynamic forces, (b) dynamic pressure forces, and (c) aerodynamic force coefficients in three directions. [M1 + aM2; a = degree of flexibility, M1 = principle mode 1; a mode of a simple flapping motion in stroke plane with 80% of total kinetic energy, and M2 = principle mode 2; a mode of wing morphing with about 15% of kinetic energy.[127]

complicated problem of the integration of vibroacoustic and aero-acoustic sounds. Hence, a thorough understanding of isolated and combined mechanisms is needed.

8. Doppler effect or the Doppler shift, which is the change in frequency or wavelength of a wave caused by a moving/stationary observer and the moving/stationary wave source, may be taken into account for the wing flexibility. Since when an insect generates a sound wave during hovering, forwarding or turning flight, it is under the Doppler effect. The knowledge of this mechanism leads to a considerable improvement in the design of biomimetic flyers, especially in military missions.

Conclusion

Since the theoretical aeroelasticity for flapping-wing aerodynamics was introduced in the 1920s, the effects of flexibility on aeroelasticity have been paid more attention to aerodynamic design. In recent years, the trait of the wing flexibility is applied for small-scale wings of biomimetic flyers including MUAVs and MAVs. So far, the growth of research and development of the flexibility effects on the aerodynamic performance and agility for these flyers with flexible wings increases through experimental and computational studies dynamically and rapidly as it is widely thought and believed that the wing flexibility should provide positive effects like biological flyers. This review on the flexibility effects on wing aerodynamics and acoustics, which is helpful to the design of biomimetic flyers, MUAVs and MAVs, is conducted up to date. Kinematics, important nondimensional parameters, and significant contribution to the flexibility effects on wing aerodynamics and acoustics are summarized and presented in table form. Overall, this review paper provides a new set of references in

acoustic investigations under the wing-flexibility effects which will be beneficial to other literature reviews in the future.

Acknowledgements

The first author would like to thank the Chinese Academy of Sciences (CAS) for giving a very good opportunity to research at the Institute of Mechanics under the PIFI post-doctoral programme. The special support of King Mongkut's Institute of Technology Ladkrabang is acknowledged as well. Finally, the authors would like to thank all researchers for their effort to contribute valuable work on the development of biomimetic flyers, MUAVs, and MAVs. The permission of using all reproduced figures in this article is acknowledged also.

Declaration of Conflicting Interests

The author(s) declared no potential conflicts of interest with respect to the research, authorship, and/or publication of this article.

Funding

The author(s) disclosed receipt of the following financial support for the research, authorship, and/or publication of this article: This paper is supported by National Key Research & Development Projects (Grant No. 2017YFB0202802), National Natural Science Foundation of China (11702297), and the Strategic Priority Research Program of the Chinese Academy of Sciences (XDB22020101).

ORCID iD

Bo Yin https://orcid.org/0000-0001-8267-8939

References

1. Birnbaum W. Das ebene problem des schlagenden flügels. *ZAMM-J Appl Math Mech/Zeitschrift für Angewandte Mathematik und Mechanik* 1924; 4: 277–292.
2. Yin, Bo, and Yang, Guowei. "Investigation of Obstacle Effects on the Aerodynamic Performance of Flapping Wings." In: *ASME 2017 fluids engineering division summer meeting*. Volume 1C, Waikoloa, Hawaii, USA. July 30–August 3, 2017. Available at DOI: 10.1115/FEDSM2017-69264.
3. Yin B, Yang G and Prapamonthon P. Finite obstacle effect on the aerodynamic performance of a hovering wing. *Phys Fluids* 2019; 31: 101902.
4. Shyy W, Aono H, Chimakurthi SK, et al. Recent progress in flapping wing aerodynamics and aeroelasticity. *Prog Aerosp Sci* 2010; 46: 284–327.
5. Helbling EF and Wood RJ. A review of propulsion, power, and control architectures for insect-scale flapping-wing vehicles. *Appl Mech Rev* 2018; 70: 010801.
6. Shyy W, Berg M and Ljungqvist D. Flapping and flexible wings for biological and micro air vehicles. *Prog Aerosp Sci* 1999; 35: 455–505.
7. Shyy W, Ifju P and Viieru D. Membrane wing-based micro air vehicles. *Appl Mech Rev* 2005; 58: 283–301.
8. Mueller TJ. *Fixed and flapping wing aerodynamics for micro air vehicle applications*. Reston, VA: American Institute of Aeronautics and Astronautics, 2001.
9. Pines DJ and Bohorquez F. Challenges facing future micro-air-vehicle development. *J Aircraft* 2006; 43: 290–305.
10. Lian Y, Shyy W, Viieru D, et al. Membrane wing aerodynamics for micro air vehicles. *Prog Aerosp Sci* 2003; 39: 425–465.
11. Platzer MF, Jones KD, Young J, et al. Flapping wing aerodynamics: progress and challenges. *AIAA J* 2008; 46: 2136–2149.
12. Ryu Y, Chang JW and Chung J. Aerodynamic characteristics of flexible wings with leading-edge veins in pitch motions. *Aerosp Sci Technol* 2019; 86: 558–571.
13. Mishra S, Tripathi B, Garg S, et al. Design and development of a bio-inspired flapping wing type micro air vehicle. *Procedia Mater Sci* 2015; 10: 519–526.
14. Nguyen AT and Han JH. Wing flexibility effects on the flight performance of an insect-like flapping-wing micro-air vehicle. *Aerosp Sci Technol* 2018; 79: 468–481.
15. Gopalakrishnan P and Tafti DK. Effect of wing flexibility on lift and thrust production in flapping flight. *AIAA J* 2010; 48: 865–877.
16. Heathcote S, Wang Z and Gursul I. Effect of spanwise flexibility on flapping wing propulsion. *J Fluids Struct* 2008; 24: 183–199.
17. Zhao L, Huang Q, Deng X, et al. Aerodynamic effects of flexibility in flapping wings. *J R Soc Interf* 2009; 7: 485–497.
18. Dai H, Luo H and Doyle JF. Dynamic pitching of an elastic rectangular wing in hovering motion. *J Fluid Mech* 2012; 693: 473–499.
19. Nakata T and Liu H. A fluid–structure interaction model of insect flight with flexible wings. *J Comput Phys* 2012; 231: 1822–1847.
20. Tian FB, Luo H, Song J, et al. Force production and asymmetric deformation of a flexible flapping wing in forward flight. *J Fluids Struct* 2013; 36: 149–161.
21. Tian FB, Young J and Lai JC. Improving power-extraction efficiency of a flapping plate: from passive deformation to active control. *J Fluids Struct* 2014; 51: 384–392.
22. Cheng X and Lan S. Effects of chordwise flexibility on the aerodynamic performance of a 3d flapping wing. *J Bionic Eng* 2015; 12: 432–442.
23. Bluman JE, Sridhar MK and Kang Ck. Chordwise wing flexibility may passively stabilize hovering insects. *J R Soc Interf* 2018; 15: 20180409.
24. Nguyen T, Sundar DS, Yeo KS, et al. Modeling and analysis of insect-like flexible wings at low Reynolds number. *J Fluids Struct* 2016; 62: 294–317.
25. Tay WB. Effect of different types of wing-wing interactions in flapping mavs. *J Bionic Eng* 2017; 14: 60–74.
26. Tobing S, Young J and Lai J. Effects of wing flexibility on bumblebee propulsion. *J Fluids Struct* 2017; 68: 141–157.
27. Zhao L, Huang Q, Deng X, et al. The effect of chordwise flexibility on the aerodynamic force generation of flapping wings: experimental studies. In: *2009 IEEE international conference on robotics and automation*. IEEE, pp.4207–4212.
28. Jankauski M, Guo Z and Shen I. The effect of structural deformation on flapping wing energetics. *J Sound Vibrat* 2018; 429: 176–192.
29. Lee N, Lee S, Cho H, et al. Effect of flexibility on flapping wing characteristics in hover and forward flight. *Comput Fluids* 2018; 173: 111–117.

30. Shahzad A, Tian FB, Young J, et al. Effects of hawkmoth-like flexibility on the aerodynamic performance of flapping wings with different shapes and aspect ratios. *Phys Fluids* 2018; 30: 091902.
31. Shahzad A, Tian FB, Young J, et al. Effects of flexibility on the hovering performance of flapping wings with different shapes and aspect ratios. *J Fluids Struct* 2018; 81: 69–96.
32. Geng B, Xue Q, Zheng X, et al. The effect of wing flexibility on sound generation of flapping wings. *Bioinspirat Biomimet* 2017; 13: 016010.
33. Chen S, Li H, Guo S, et al. Unsteady aerodynamic model of flexible flapping wing. *Aerosp Sci Technol* 2018; 80: 354–367.
34. Dickinson MH and Gotz KG. Unsteady aerodynamic performance of model wings at low Reynolds numbers. *J Exp Biol* 1993; 174: 45–64.
35. Ellington CP, Van Den Berg C, Willmott AP, et al. Leading-edge vortices in insect flight. *Nature* 1996; 384: 626.
36. Bhayu PR, Nguyen QV, Park HC, et al. Artificial cambered-wing for a beetle-mimicking flapper. *J Bionic Eng* 2010; 7: S130–S136.
37. Combes S and Daniel T. Flexural stiffness in insect wings i. scaling and the influence of wing venation. *J Exp Biol* 2003; 206: 2979–2987.
38. Combes S and Daniel T. Flexural stiffness in insect wings ii. spatial distribution and dynamic wing bending. *J Exp Biol* 2003; 206: 2989–2997.
39. Wehmann HN, Heepe L, Gorb SN, et al. Local deformation and stiffness distribution in fly wings. *Biol Open* 2019; 8bio038299.
40. Tanaka H, Whitney JP and Wood RJ. Effect of flexural and torsional wing flexibility on lift generation in hoverfly flight. *Integrative and Comparative Biology* 2011; 51: 142–150.
41. San Ha N, Truong QT, Goo NS, et al. Biomechanical properties of insect wings: the stress stiffening effects on the asymmetric bending of the allomyrina dichotoma beetle's hind wing. *PloS One* 2013; 8: e80689.
42. Sivasankaran PN, Ward TA, Salami E, et al. An experimental study of elastic properties of dragonfly-like flapping wings for use in biomimetic micro air vehicles (bmavs). *Chin J Aeronaut* 2017; 30: 726–737.
43. Yin B and Luo H. Effect of wing inertia on hovering performance of flexible flapping wings. *Phys Fluids* 2010; 22: 111902.
44. Abas MFB, Rafie ASBM, Yusoff HB, et al. Flapping wing micro-aerial-vehicle: kinematics, membranes, and flapping mechanisms of ornithopter and insect flight. *Chin J Aeronaut* 2016; 29: 1159–1177.
45. Weidenfeld M and Manela A. The effect of flexural stiffness on the sound of a hanging filament: from a membrane to a rigid body. *J Sound Vibrat* 2018; 433: 65–76.
46. Purohit A, Darpe AK and Singh S. A numerical investigation on effects of structural flexibility on aerodynamic far field sound. *Comput Fluids* 2014; 89: 143–152.
47. Manela A. Sound generated by a vortex convected past an elastic sheet. *J Sound Vibrat* 2011; 330: 416–430.
48. Shyy W, Lian Y, Tang J, et al. *Aerodynamics of low Reynolds number flyers*. New York: Cambridge University Press, 2007. volume 22.
49. Willmott AP and Ellington CP. The mechanics of flight in the hawkmoth manduca sexta. i. kinematics of hovering and forward flight. *J Exp Biol* 1997; 200: 2705–2722.
50. Liu H. Integrated modeling of insect flight: from morphology, kinematics to aerodynamics. *J Comput Phys* 2009; 228: 439–459.
51. Liu H, Ellington CP, Kawachi K, et al. A computational fluid dynamic study of hawkmoth hovering. *J Exp Biol* 1998; 201: 461–477.
52. Bos FM, Lentink D, Van Oudheusden B, et al. Influence of wing kinematics on aerodynamic performance in hovering insect flight. *J Fluid Mech* 2008; 594: 341–368.
53. Sane SP and Dickinson MH. The control of flight force by a flapping wing: lift and drag production. *J Exp Biol* 2001; 204: 2607–2626.
54. Wootton RJ. Functional morphology of insect wings. *Ann Rev Entomol* 1992; 37: 113–140.
55. Hodges D, Pierce G and Cutchins M. Introduction to structural dynamics and aeroelasticity. *ASME Appl Mech Rev* 2003; 56: B35. Available at DOI: 10.1115/1.1566393.
56. Jones K, Dohring C and Platzer M. Experimental and computational investigation of the Knoller-Betz effect. *AIAA J* 1998; 36: 1240–1246.
57. Aono H, Chimakurthi S, Cesnik C, et al. Computational modeling of spanwise flexibility effects on flapping wing aerodynamics. In: *47th AIAA aerospace sciences meeting including the new horizons forum and aerospace exposition*. p. 1270.
58. Guerrero JE. *Numerical simulation of the unsteady aerodynamics of flapping flight*. PhD Thesis, University of Genoa, Genova, 2009.
59. Wang ZJ. Vortex shedding and frequency selection in flapping flight. *J Fluid Mech* 2000; 410: 323–341.
60. Triantafyllou M, Triantafyllou G and Gopalkrishnan R. Wake mechanics for thrust generation in oscillating foils. *Phys Fluids A: Fluid Dyn* 1991; 3: 2835–2837.
61. Taylor GK, Nudds RL and Thomas AL. Flying and swimming animals cruise at a Strouhal number tuned for high power efficiency. *Nature* 2003; 425: 707.
62. Nudds RL, Taylor GK and Thomas AL. Tuning of Strouhal number for high propulsive efficiency accurately predicts how wingbeat frequency and stroke amplitude relate and scale with size and flight speed in birds. *Proc R Soc Lond Series B Biol Sci* 2004; 271: 2071–2076.
63. Triantafyllou MS, Triantafyllou G and Yue D. Hydrodynamics of fishlike swimming. *Ann Rev Fluid Mech* 2000; 32: 33–53.
64. Tanaka H, Okada H, Shimasue Y, et al. Flexible flapping wings with self-organized microwrinkles. *Bioinspirat Biomimet* 2015; 10: 046005.
65. Timoshenko S. *Theory of elastic stability*. New York: McGraw Hill, 1961.
66. Fu J, Liu X, Shyy W, et al. Effects of flexibility and aspect ratio on the aerodynamic performance of flapping wings. *Bioinspirat Biomimet* 2018; 13: 036001.
67. Anderson J. *Fundamentals of aerodynamics*. New York: McGraw Hill, 2001.
68. Fletcher CA. *Computational techniques for fluid dynamics 2: Specific techniques for different flow*

categories. New York: Springer Science & Business Media, 2012.
69. Ghorbel O, Casimir JB, Hammami L, et al. Dynamic stiffness formulation for free orthotropic plates. *J Sound Vibrat* 2015; 346: 361–375.
70. Damnjanović E, Nefovska-Danilović M, Petronijević M, et al. Application of the dynamic stiffness method in the vibration analysis of stiffened composite plates. *Proc Eng* 2017; 199: 224–229.
71. Axisa F and Trompette P. *Modelling of mechanical systems: structural elements*. Oxford: Elsevier, 2005 volume 2.
72. Christensen RM. *Mechanics of composite materials*. North Chelmsford: Courier Corporation, 2012.
73. Reddy JN. *Mechanics of laminated composite plates and shells: theory and analysis*. Boca Raton: CRC Press, 2003.
74. Yang W, Song B, Song W, et al. The effects of spanwise and chord-wise flexibility on the aerodynamic performance of micro flapping-wing. *Chin Sci Bull* 2012; 57: 2887–2897.
75. Kang W, Zhang Jz, Lei Pf, et al. Computation of unsteady viscous flow around a locally flexible airfoil at low Reynolds number. *J Fluids Struct* 2014; 46: 42–58.
76. Lehmann FO, Gorb S, Nasir N, et al. Elastic deformation and energy loss of flapping fly wings. *J Exp Biol* 2011; 214: 2949–2961.
77. Luo H, Tian F, Song J, et al. Aerodynamic cause of the asymmetric wing deformation of insect wings. In: *APS Meeting Abstracts*, *APS Division of Fluid Dynamics (Fall)* 2012; abstract id. E32.003.
78. Heathcote S, Martin D and Gursul I. Flexible flapping airfoil propulsion at zero freestream velocity. *AIAA J* 2004; 42: 2196–2204.
79. Heathcote S and Gursul I. Flexible flapping airfoil propulsion at low reynolds numbers. *AIAA J* 2007; 45: 1066–1079.
80. Miao JM and Ho MH. Effect of flexure on aerodynamic propulsive efficiency of flapping flexible airfoil. *J Fluids Struct* 2006; 22: 401–419.
81. Zhu Q. Numerical simulation of a flapping foil with chordwise or spanwise flexibility. *AIAA J* 2007; 45: 2448–2457.
82. Unger R, Haupt MC, Horst P, et al. Fluid–structure analysis of a flexible flapping airfoil at low Reynolds number flow. *J Fluids Struct* 2012; 28: 72–88.
83. Ulrich X and Peters D. Loads and propulsive efficiency of a flexible airfoil performing sinusoidal deformations. *J Fluids Struct* 2014; 45: 15–27.
84. Kinsey T and Dumas G. Parametric study of an oscillating airfoil in a power-extraction regime. *AIAA J* 2008; 46: 1318–1330.
85. Zhu Q. Energy harvesting by a purely passive flapping foil from shear flows. *J Fluids Struct* 2012; 34: 157–169.
86. Young J, Ashraf MA, Lai JC, et al. Numerical simulation of fully passive flapping foil power generation. *AIAA J* 2013; 51: 2727–2739.
87. Wu J, Wu J, Tian FB, et al. How a flexible tail improves the power extraction efficiency of a semi-activated flapping foil system: a numerical study. *J Fluids Struct* 2015; 54: 886–899.
88. Chimakurthi SK, Tang J, Palacios R, et al. Computational aeroelasticity framework for analyzing flapping wing micro air vehicles. *AIAA J* 2009; 47: 1865–1878.
89. Hu H, Kumar AG, Abate G, et al. An experimental investigation on the aerodynamic performances of flexible membrane wings in flapping flight. *Aerosp Sci Technol* 2010; 14: 575–586.
90. Nakata T, Liu H, Tanaka Y, et al. Aerodynamics of a bio-inspired flexible flapping-wing micro air vehicle. *Bioinspirat Biomimet* 2011; 6: 045002.
91. Lu G, Yan J, Zhang Z, et al. Dissection of a flexible wing's performance for insect-inspired flapping-wing micro air vehicles. *Adv Robot* 2012; 26: 409–435.
92. Mountcastle AM and Combes SA. Wing flexibility enhances load-lifting capacity in bumblebees. *Proc R Soc B Biol Sci* 2013; 280: 20130531.
93. Agrawal A and Agrawal SK. Design of bio-inspired flexible wings for flapping-wing micro-sized air vehicle applications. *Adv Robot* 2009; 23: 979–1002.
94. Wu P, Stanford B, Sällström E, et al. Structural dynamics and aerodynamics measurements of biologically inspired flexible flapping wings. *Bioinspirat Biomimet* 2011; 6: 016009.
95. Nagai H, Isogai K, Fujimoto T, et al. Experimental and numerical study of forward flight aerodynamics of insect flapping wing. *AIAA J* 2009; 47: 730–742.
96. Deng S, Percin M, van Oudheusden B, et al. Numerical simulation of a flexible x-wing flapping-wing micro air vehicle. *AIAA J* 2017; 55: 2295–2306.
97. Jadhav S, Lua K and Tay W. Effect of clap-and-fling mechanism on force generation in flapping wing micro aerial vehicles. *Bioinspirat Biomimet* 2019; 14: 036006.
98. Pourtakdoust S and Aliabadi SK. Evaluation of flapping wing propulsion based on a new experimentally validated aeroelastic model. *Scientia Iranica* 2012; 19: 472–482.
99. Mazaheri K and Ebrahimi A. Experimental investigation on aerodynamic performance of a flapping wing vehicle in forward flight. *J Fluids Struct* 2011; 27: 586–595.
100. Du G and Sun M. Effects of wing deformation on aerodynamic forces in hovering hoverflies. *J Exp Biol* 2010; 213: 2273–2283.
101. Medina A, Eldredge JD, Kweon J, et al. Illustration of wing deformation effects in three-dimensional flapping flight. *AIAA J* 2015; 53: 2607–2620.
102. Drosopoulos S and Claridge M. *Insect sound and communication, physiology, behavior, ecology, and evolution*. Boca Raton: CRC Press, 2006.
103. Sueur J, Tuck EJ and Robert D. Sound radiation around a flying fly. *J Acoust Soc Am* 2005; 118: 530–538.
104. Inada Y, Aono H, Liu H, et al. Numerical analysis of sound generation of insect flapping wings. *Theoret Appl Mech Jpn* 2009; 57: 437–447.
105. Seo JH, Hedrick T and Mittal R. Mechanism and scaling of wing tone generation in mosquitoes. *Bioinspirat Biomimet* 2019; 15: 016008.
106. Van Den Berg C and Ellington CP. The vortex wake of a hoveringmodel hawkmoth. *Phil Trans R Soc Lond Series B Biol Sci* 1997; 352: 317–328.

107. Sane SP. The aerodynamics of insect flight. *J Exp Biol* 2003; 206: 4191–4208.
108. Wang L and Tian FB. Numerical study of flexible flapping wings with an immersed boundary method: fluid–structure–acoustics interaction. *J Fluids Struct* 2019; 90: 396–409.
109. Lighthill M. On sound generated aerodynamically i. general theory. *Proc R Soc A* 1952; 211: 564–587.
110. Ffowcs Williams JE and Hawkings DL. Sound generation by turbulence and surfaces in arbitrary motion. *Phil Trans R Soc Lond Series A Math Phys Sci* 1969; 264: 321–342.
111. Schlanderer S, Weymouth G and Sandberg R. The boundary data immersion method for compressible flows with application to aeroacoustics. *J Comput Phys* 2017; 333: 440–461.
112. Hardin J and Pope D. An acoustic/viscous splitting technique for computational aeroacoustics. *Theoret Computat Fluid Dyn* 1994; 6: 323–340.
113. Nedunchezian K, Kang Ck and Aono H. Effects of flapping wing kinematics on the aeroacoustics of hovering flight. *J Sound Vibrat* 2019; 442: 366–383.
114. Guo Y. Application of the Ffowcs Williams/Hawkings equation to two-dimensional problems. *J Fluid Mech* 2000; 403: 201–221.
115. Manoha E, Herrero C, Sagaut P, et al. Numerical prediction of airfoil aerodynamic noise. In: 8th AIAA/CEAS Aeroacoustics Conference & Exhibit 17 June 2002 – 19 June 2002, Breckenridge, Colorado. *AIAA Paper* 2002; 2002–2573. DOI: 10.2514/6.2002-2573.
116. Sandberg R and Sandham N. Direct numerical simulation of turbulent flow past a trailing edge and the associated noise generation. *J Fluid Mech* 2008; 596: 353–385.
117. Wang L, Tian FB and Lai J. An immersed boundary method for fluidstructureacoustics interactions involving large deformations and complex geometries. *arXiv preprint arXiv:190500182*.
118. Goldstein D, Handler R and Sirovich L. Modeling a no-slip flow boundary with an external force field. *J Computat Phys* 1993; 105: 354–366.
119. Peskin CS. The immersed boundary method. *Acta Numerica* 2002; 11: 479–517.
120. Purohit A, Darpe AK and Singh S. A study on aerodynamic sound from an externally excited flexible structure in flow. *Comput Fluids* 2014; 103: 100–115.
121. Manela A. Vibration and sound of an elastic wing actuated at its leading edge. *J Sound Vibrat* 2012; 331: 638–650.
122. Manela A and Halachmi M. Mechanisms of sound amplification and sound reduction in the flapping flight of side-by-side airfoils. *J Sound Vibrat* 2015; 346: 216–228.
123. Jaworski JW and Peake N. Aerodynamic noise from a poroelastic edge with implications for the silent flight of owls. *J Fluid Mech* 2013; 723: 456–479.
124. Springer M, Scheit C and Becker S. Fluid-structure-acoustic coupling for a flat plate. *Int J Heat Fluid Flow* 2017; 66: 249–257.
125. Nedunchezian K, Kang Ck and Aono H. Sound generation of flexible plunging wings in hover at low Reynolds numbers. In: *AIAA Scitech 2019 Forum*, 7–11 January 2019, San Diego, California, p.1072. DOI: 10.2514/6.2019-1072.
126. Meng XG, Liu YP and Sun M. Aerodynamics of ascending flight in fruit flies. *J Bionic Eng* 2017; 14: 75–87.
127. Geng B, Zheng X, Xue Q, et al. A numerical study of the sound and force production of flexible insect wings. *Fluids* 2018; 3: 87.
128. Yusoff JE. *Experimental and numerical investigations on the performance of flexible skin flapping wing for micro aerial vehicle application*. PhD Thesis, Universiti Sains Malaysia, Gelugor, Penang, 2013.
129. Deng HB, Xu YQ, Chen DD, et al. On numerical modeling of animal swimming and flight. *Computat Mech* 2013; 52: 1221–1242.
130. Huang WX and Tian FB. Recent trends and progresses in the immersed boundary method. *Proc IMechE, Part C: J Mechanical Engineering Science* 2019; 23–24: 7617–7636.
131. Brambley E. Optimized finite-difference (drp) schemes perform poorly for decaying or growing oscillations. *J Computat Phys* 2016; 324: 258–274.
132. Haras Z and Ta'asan S. Finite difference schemes for long-time integration. *J Computat Phys* 1994; 114: 265–279.
133. Sjgreen B and Yee HC. Accuracy consideration by DRP schemes for DNS and les of compressible flow computations. *Comput Fluids* 2017; 159: 123–136.